

Nucleosynthesis Basics and Applications to Supernovae

By F.-K. THIELEMANN^{1,5},
 T. RAUSCHER¹,
 C. FREIBURGHHAUS^{1,5}, K. NOMOTO^{2,5},
 M. HASHIMOTO³,
 B. PFEIFFER⁴ AND K.-L. KRATZ⁴

¹Departement für Physik und Astronomie, Universität Basel, CH-4056 Basel, Switzerland

²Department of Astronomy and Research Center for the Early Universe, University of Tokyo, Tokyo 113, Japan

³Department of Physics, Faculty of Science, Kyushu University, Fukuoka 810, Japan

⁴Institut für Kernchemie, Universität Mainz, D-55128 Mainz, Germany

⁵Institute for Theoretical Physics, University of California, Santa Barbara, CA 93106-4030

This review concentrates on nucleosynthesis processes in general and their applications to massive stars and supernovae. A brief initial introduction is given to the physics in astrophysical plasmas which governs composition changes. We present the basic equations for thermonuclear reaction rates and nuclear reaction networks. The required nuclear physics input for reaction rates is discussed, i.e. cross sections for nuclear reactions, photodisintegrations, electron and positron captures, neutrino captures, inelastic neutrino scattering, and beta-decay half-lives. We examine especially the present state of uncertainties in predicting thermonuclear reaction rates, while the status of experiments is discussed by others in this volume (see M. Wiescher). It follows a brief review of hydrostatic burning stages in stellar evolution before discussing the fate of massive stars, i.e. the nucleosynthesis in type II supernova explosions (SNe II). Except for SNe Ia, which are explained by exploding white dwarfs in binary stellar systems (which will not be discussed here), all other supernova types seem to be linked to the gravitational collapse of massive stars ($M > 8M_{\odot}$) at the end of their hydrostatic evolution. SN1987A, the first type II supernova for which the progenitor star was known, is used as an example for nucleosynthesis calculations. Finally, we discuss the production of heavy elements in the r-process up to Th and U and its possible connection to supernovae.

1. Thermonuclear Rates and Reaction Networks

In this section we want to outline the essential features of thermonuclear reaction rates and nuclear reaction networks. This serves the purpose to define a unified terminology to be used throughout the review, more detailed discussions can be found in Fowler, Caughlan, & Zimmerman (1967,1975), Clayton (1983), Rolfs & Rodney (1988), Thielemann, Nomoto, & Hashimoto (1994), and Arnett (1996).

1.1. Thermonuclear Reaction Rates

The nuclear cross section for a reaction between target j and projectile k is defined by

$$\sigma = \frac{\text{number of reactions target}^{-1}\text{sec}^{-1}}{\text{flux of incoming projectiles}} = \frac{r/n_j}{n_k v}. \quad (1.1)$$

The second equality holds for the case that the relative velocity between targets with the number density n_j and projectiles with number density n_k is constant and has the value v . Then r , the number of reactions per cm^3 and sec, can be expressed as $r = \sigma v n_j n_k$. More generally, when targets and projectiles follow specific distributions, r is given by

$$r_{j,k} = \int \sigma |\vec{v}_j - \vec{v}_k| d^3 n_j d^3 n_k. \quad (1.2)$$

The evaluation of this integral depends on the type of particles and distributions which are involved. For nuclei j and k in an astrophysical plasma, obeying a Maxwell-Boltzmann distribution,

$$d^3 n_j = n_j \left(\frac{m_j}{2\pi kT} \right)^{3/2} \exp\left(-\frac{m_j v_j^2}{2kT}\right) d^3 v_j, \quad (1.3)$$

Eq.(1.2) simplifies to $r_{j,k} = \langle \sigma v \rangle n_j n_k$. The thermonuclear reaction rates have the form (Fowler, Caughlan, & Zimmerman 1967, Clayton 1983)

$$r_{j,k} = \langle \sigma v \rangle_{j,k} n_j n_k \quad (1.4a)$$

$$\langle j, k \rangle = \langle \sigma v \rangle_{j,k} = \left(\frac{8}{\mu\pi} \right)^{1/2} (kT)^{-3/2} \int_0^\infty E \sigma(E) \exp(-E/kT) dE. \quad (1.4b)$$

Here μ denotes the reduced mass of the target-projectile system. In astrophysical plasmas with high densities and/or low temperatures, effects of electron screening become highly important. This means that the reacting nuclei, due to the background of electrons and nuclei, feel a different Coulomb repulsion than in the case of bare nuclei. Under most conditions (with non-vanishing temperatures) the generalized reaction rate integral can be separated into the traditional expression without screening [Eq.(1.4)] and a screening factor (see e.g. Salpeter & van Horn 1969, Itoh, Totsuji, & Ichimaru 1977, Hansen, Torrie, & Veillefosse 1977, Alastuey & Jancovici 1978, Itoh et al. 1979, Ichimaru, Tanaka, Iyetomi 1984, Ichimaru & Utsumi 1983, 1984, Thielemann & Truran 1987, Fushiki & Lamb 1987, Itoh et al. 1990, Schramm & Koonin 1990, Ichimaru 1993, Chabrier & Schatzman 1994, Kitamura & Ichimaru 1995, Brown & Sawyer 1997)

$$\langle j, k \rangle^* = f_{scr}(Z_j, Z_k, \rho, T, Y_i) \langle j, k \rangle. \quad (1.5)$$

This screening factor is dependent on the charge of the involved particles, the density, temperature, and the composition of the plasma. Here Y_i denotes the abundance of nucleus i defined by $Y_i = n_i / (\rho N_A)$, where n_i is the number density of nuclei per unit volume and N_A Avogadro's number. At high densities and low temperatures screening factors can enhance reactions by many orders of magnitude and lead to *pycnonuclear ignition*. In the extreme case of very low temperatures, where reactions are only possible via ground state oscillations of the nuclei in a Coulomb lattice, Eq.(1.5) breaks down, because it was derived under the assumption of a Boltzmann distribution (for recent references see Fushiki & Lamb 1987, Itoh et al. 1990, Schramm & Koonin 1990, Ichimaru 1993, Chabrier & Schatzman 1994, Ichimaru 1996).

When in Eq.(1.2) particle k is a photon, the relative velocity is always c and quantities in the integral are not dependent on $d^3 n_j$. Thus it simplifies to $r_j = \lambda_{j,\gamma} n_j$ and $\lambda_{j,\gamma}$ results from an integration of the photodisintegration cross section over a Planck distribution for photons of temperature T

$$d^3 n_\gamma = \frac{1}{\pi^2 (c\hbar)^3} \frac{E_\gamma^2}{\exp(E_\gamma/kT) - 1} dE_\gamma \quad (1.6a)$$

$$r_j = \lambda_{j,\gamma}(T) n_j = \frac{\int d^3 n_j}{\pi^2 (c\hbar)^3} \int_0^\infty \frac{c \sigma(E_\gamma) E_\gamma^2}{\exp(E_\gamma/kT) - 1} dE_\gamma. \quad (1.6b)$$

There is, however, no direct need to evaluate photodisintegration cross sections, because, due to detailed balance, they can be expressed by the capture cross sections for the inverse reaction $l + m \rightarrow j + \gamma$ (Fowler et al. 1967)

$$\lambda_{j,\gamma}(T) = \left(\frac{G_l G_m}{G_j}\right) \left(\frac{A_l A_m}{A_j}\right)^{3/2} \left(\frac{m_u kT}{2\pi\hbar^2}\right)^{3/2} \langle l, m \rangle \exp(-Q_{lm}/kT). \quad (1.7)$$

This expression depends on the reaction Q-value Q_{lm} , the temperature T , the inverse reaction rate $\langle l, m \rangle$, the partition functions $G(T) = \sum_i (2J_i + 1) \exp(-E_i/kT)$ and the mass numbers A of the participating nuclei in a thermal bath of temperature T .

A procedure similar to Eq.(1.6) is used for electron captures by nuclei. Because the electron is about 2000 times less massive than a nucleon, the velocity of the nucleus j is negligible in the center of mass system in comparison to the electron velocity ($|\vec{v}_j - \vec{v}_e| \approx |\vec{v}_e|$). The electron capture cross section has to be integrated over a Boltzmann, partially degenerate, or Fermi distribution of electrons, dependent on the astrophysical conditions. The electron capture rates are a function of T and $n_e = Y_e \rho N_A$, the electron number density (Fuller, Fowler, & Newman 1980, 1982, 1985). In a neutral, completely ionized plasma, the electron abundance is equal to the total proton abundance in nuclei $Y_e = \sum_i Z_i Y_i$ and

$$r_j = \lambda_{j,e}(T, \rho Y_e) n_j. \quad (1.8)$$

The same authors generalized this treatment for the capture of positrons, which are in a thermal equilibrium with photons, electrons, and nuclei. At high densities ($\rho > 10^{12} \text{gcm}^{-3}$) the size of the neutrino scattering cross section on nuclei and electrons ensures that enough scattering events occur to thermalize a neutrino distribution. Then also the inverse process to electron capture (neutrino capture) can occur and the neutrino capture rate can be expressed similar to Eqs.(1.6) or (1.8), integrating over the neutrino distribution (e.g. Fuller & Meyer 1995). Also inelastic neutrino scattering on nuclei can be expressed in this form. The latter can cause particle emission, like in photodisintegrations (e.g. Woosley et al. 1990, Kolbe et al. 1992, 1993, 1995, Qian et al. 1996). It is also possible that a thermal equilibrium among neutrinos was established at a different location than at the point where the reaction occurs. In such a case the neutrino distribution can be characterized by a chemical potential and a temperature which is not necessarily equal to the local temperature. Finally, for normal decays, like beta or alpha decays with half-life $\tau_{1/2}$, we obtain an equation similar to Eqs.(1.6) or (1.8) with a decay constant $\lambda_j = \ln 2/\tau_{1/2}$ and

$$r_j = \lambda_j n_j. \quad (1.9)$$

1.2. Nuclear Reaction Networks

The time derivative of the number densities of each of the species in an astrophysical plasma (at constant density) is governed by the different expressions for r , the number of reactions per cm^3 and sec, as discussed above for the different reaction mechanisms which can change nuclear abundances

$$\left(\frac{\partial n_i}{\partial t}\right)_{\rho=\text{const}} = \sum_j N_j^i r_j + \sum_{j,k} N_{j,k}^i r_{j,k} + \sum_{j,k,l} N_{j,k,l}^i r_{j,k,l}. \quad (1.10)$$

The reactions listed on the right hand side of the equation belong to the three categories of reactions: (1) decays, photodisintegrations, electron and positron captures and

neutrino induced reactions ($r_j = \lambda_j n_j$), (2) two-particle reactions ($r_{j,k} = \langle j, k \rangle n_j n_k$), and (3) three-particle reactions ($r_{j,k,l} = \langle j, k, l \rangle n_j n_k n_l$) like the triple-alpha process, which can be interpreted as successive captures with an intermediate unstable target (see e.g. Nomoto, Thielemann, & Miyaji 1985, Görres, Wiescher, & Thielemann 1995). The individual N^i 's are given by: $N_j^i = N_i$, $N_{j,k}^i = N_i / \prod_{m=1}^{n_m} |N_{j_m}^i|$, and $N_{j,k,l}^i = N_i / \prod_{m=1}^{n_m} |N_{j_m}^i|$. The N^i 's can be positive or negative numbers and specify how many particles of species i are created or destroyed in a reaction. The denominators, including factorials, run over the n_m different species destroyed in the reaction and avoid double counting of the number of reactions when identical particles react with each other (for example in the $^{12}\text{C}+^{12}\text{C}$ or the triple-alpha reaction; for details see Fowler et al. 1967). In order to exclude changes in the number densities \hat{n}_i , which are only due to expansion or contraction of the gas, the nuclear abundances $Y_i = n_i / (\rho N_A)$ were introduced. For a nucleus with atomic weight A_i , $A_i Y_i$ represents the mass fraction of this nucleus, therefore $\sum A_i Y_i = 1$. In terms of nuclear abundances Y_i , a reaction network is described by the following set of differential equations

$$\dot{Y}_i = \sum_j N_j^i \lambda_j Y_j + \sum_{j,k} N_{j,k}^i \rho N_A \langle j, k \rangle Y_j Y_k + \sum_{j,k,l} N_{j,k,l}^i \rho^2 N_A^2 \langle j, k, l \rangle Y_j Y_k Y_l. \quad (1.11)$$

Eq.(1.11) derives directly from Eq.(1.10) when the definition for the Y_i 's is introduced. This set of differential equations is solved with a fully implicit treatment. Then the stiff set of differential equations can be rewritten (see e.g. Press et al. 1986, §15.6) as difference equations of the form $\Delta Y_i / \Delta t = f_i(Y_j(t + \Delta t))$, where $Y_i(t + \Delta t) = Y_i(t) + \Delta Y_i$. In this treatment, all quantities on the right hand side are evaluated at time $t + \Delta t$. This results in a set of non-linear equations for the new abundances $Y_i(t + \Delta t)$, which can be solved using a multi-dimensional Newton-Raphson iteration procedure. The total energy generation per gram, due to nuclear reactions in a time step Δt which changed the abundances by ΔY_i , is expressed in terms of the mass excess $M_{ex,i} c^2$ of the participating nuclei (Audi & Wapstra 1995)

$$\Delta \epsilon = - \sum_i \Delta Y_i N_A M_{ex,i} c^2 \quad (1.12a)$$

$$\dot{\epsilon} = - \sum_i \dot{Y}_i N_A M_{ex,i} c^2. \quad (1.12b)$$

As noted above, the important ingredients to nucleosynthesis calculations are decay half-lives, electron and positron capture rates, photodisintegrations, neutrino induced reaction rates, and strong interaction cross sections. Beta-decay half-lives for unstable nuclei have been predicted by Takahashi, Yamada, & Kondo (1973), Klapdor, Metzinger, & Oda (1984), Takahashi & Yokoi (1987, also including temperature effects) and more recently with improved quasi particle RPA calculations (Staudt et al. 1989, 1990, Möller & Randrup 1990, Hirsch et al. 1992, Pfeiffer & Kratz 1996, Möller, Nix, & Kratz 1997, Borzov 1996, 1997). Electron and positron capture calculations have been performed by Fuller, Fowler, & Newman (1980, 1982, 1985) for a large variety of nuclei with mass numbers between $A=20$ and $A=60$. For revisions see also Takahara et al. (1989) and for heavier nuclei Aufderheide et al. (1994), Sutaria, Sheikh, & Ray (1997). Rates for inelastic neutrino scattering have been presented by Woosley et al. (1990) and Kolbe et al. (1992, 1993, 1995). Photodisintegration rates can be calculated via detailed balance from the reverse capture rates. Experimental nuclear rates for light nuclei have been discussed in detail in the reviews by Rolfs, Trautvetter, & Rodney (1987), Filippone (1987), the book by Rolfs & Rodney (1988), the recent review on 40 years after B²FH by Wallerstein

et al. (1997), and the NuPECC report on nuclear and particle astrophysics (Baraffe et al. 1997). The most recent experimental charged particle rate compilations are the ones by Caughlan & Fowler (1988) and Arnould et al. (1997). Experimental neutron capture cross sections are summarized by Bao & Käppeler (1987, 1997), Beer, Voss, & Winters (1992), and Wisshak et al. (1997). Rates for unstable (light) nuclei are given by Malaney & Fowler (1988, 1989), Wiescher et al. (1986, 1987, 1988ab, 1989ab, 1990), Thomas et al. (1993,1994), van Wormer et al. (1994), Rauscher et al. (1994), and Schatz et al. (1997). For additional information see the article by M. Wiescher (this volume). For the vast number of medium and heavy nuclei which exhibit a high density of excited states at capture energies, Hauser-Feshbach (statistical model) calculations are applicable. The most recent compilations were provided by Holmes et al. (1975), Woosley et al. (1978), and Thielemann, Arnould, & Truran (1987, for a detailed discussion of the methods involved and neutron capture cross sections for heavy unstable nuclei see also section 3.4 and the appendix in Cowan, Thielemann, Truran 1991). Improvements in level densities (Rauscher, Thielemann, & Kratz 1997), alpha potentials, and the consistent treatment of isospin mixing will lead to the next generation of theoretical rate predictions (Rauscher et al. 1998). Some of it will be discussed in the following section.

2. Theoretical Cross Section Predictions

Explosive nuclear burning in astrophysical environments produces unstable nuclei, which again can be targets for subsequent reactions. In addition, it involves a very large number of stable nuclei, which are not fully explored by experiments. Thus, it is necessary to be able to predict reaction cross sections and thermonuclear rates with the aid of theoretical models. Explosive burning in supernovae involves in general intermediate mass and heavy nuclei. Due to a large nucleon number they have intrinsically a high density of excited states. A high level density in the compound nucleus at the appropriate excitation energy allows to make use of the statistical model approach for compound nuclear reactions [e.g. Hauser & Feshbach (1952), Mahaux & Weidenmüller (1979), Gadioli & Hodgson (1992)] which averages over resonances. Here, we want to present recent results obtained within this approach and outline in a clear way, where in the nuclear chart and for which environment temperatures its application is valid. It is often colloquially termed that the statistical model is only applicable for intermediate and heavy nuclei. However, the only necessary condition for its application is a large number of resonances at the appropriate bombarding energies, so that the cross section can be described by an average over resonances. This can in specific cases be valid for light nuclei and on the other hand not be valid for intermediate mass nuclei near magic numbers.

In astrophysical applications usually different aspects are emphasized than in pure nuclear physics investigations. Many of the latter in this long and well established field were focused on specific reactions, where all or most "ingredients", like optical potentials for particle and alpha transmission coefficients, level densities, resonance energies and widths of giant resonances to be implemented in predicting E1 and M1 gamma-transitions, were deduced from experiments. This of course, as long as the statistical model prerequisites are met, will produce highly accurate cross sections. For the majority of nuclei in astrophysical applications such information is not available. The real challenge is thus not the well established statistical model, but rather to provide all these necessary ingredients in as reliable a way as possible, also for nuclei where none of such informations are available. In addition, these approaches should be on a similar level as e.g. mass models, where the investigation of hundreds or thousands of nuclei is possible

with manageable computational effort, which is not always the case for fully microscopic calculations.

The statistical model approach has been employed in calculations of thermonuclear reaction rates for astrophysical purposes by many researchers [Truran et al. (1966), Michaud & Fowler (1970, 1972), Truran (1972)], who in the beginning only made use of ground state properties. Later, the importance of excited states of the target was pointed out by Arnould (1972). The compilations by Holmes et al. (1976), Woosley et al. (1978), Thielemann et al. (1987), and Cowan, Thielemann & Truran (1991) are presently the ones utilized in large scale applications in all subfields of nuclear astrophysics, when experimental information is unavailable. Existing global optical potentials, mass models to predict Q-values, deformations etc., but also the ingredients to describe giant resonance properties have been quite successful in the past [see e.g. the review by Cowan et al. (1991)].

Besides possibly necessary improvements in global alpha potentials (see Mohr et al. 1997), the major remaining uncertainty in all existing calculations stems from the prediction of nuclear level densities, which in earlier calculations gave uncertainties even beyond a factor of 10 at the neutron separation energy for Gilbert & Cameron (1965), about a factor of 8 for Woosley et al. (1978), and a factor of 5 even in the most recent calculations [e.g. Thielemann et al. (1987); see Fig.3.16 in Cowan et al. (1991)]. In nuclear reactions the transitions to lower lying states dominate due to the strong energy dependence. Because the deviations are usually not as high yet at low excitation energies, the typical cross section uncertainties amounted to a smaller factor of 2–3.

The implementation of a novel treatment of level density descriptions Iljinov et al. (1992), Ignatyuk et al. (1979), where the level density parameter is energy dependent and shell effects vanish at high excitation energies, improves the level density accuracy. This is still a phenomenological approach, making use of a back-shifted Fermi-gas model rather than a combinatorial approach based on microscopic single-particle levels. But it is the first one leading to a reduction of the average cross section uncertainty to a factor of about 1.4, i.e. an average deviation of about 40% from experiments, when only employing global predictions for all input parameters and no specific experimental knowledge.

2.1. Thermonuclear Rates from Statistical Model Calculations

A high level density in the compound nucleus permits to use averaged transmission coefficients T , which do not reflect a resonance behavior, but rather describe absorption via an imaginary part in the (optical) nucleon-nucleus potential as described in Mahaux & Weidenmüller (1979). This leads to the well known expression

$$\sigma_i^{\mu\nu}(j, o; E_{ij}) = \frac{\pi \hbar^2 / (2\mu_{ij} E_{ij})}{(2J_i^\mu + 1)(2J_j + 1)} \times \sum_{J, \pi} (2J + 1) \frac{T_j^\mu(E, J, \pi, E_i^\mu, J_i^\mu, \pi_i^\mu) T_o^\nu(E, J, \pi, E_m^\nu, J_m^\nu, \pi_m^\nu)}{T_{tot}(E, J, \pi)} \quad (2.13)$$

for the reaction $i^\mu(j, o)m^\nu$ from the target state i^μ to the excited state m^ν of the final nucleus, with a center of mass energy E_{ij} and reduced mass μ_{ij} . J denotes the spin, E the corresponding excitation energy in the compound nucleus, and π the parity of excited states. When these properties are used without subscripts they describe the compound nucleus, subscripts refer to states of the participating nuclei in the reaction $i^\mu(j, o)m^\nu$ and superscripts indicate the specific excited states. Experiments measure $\sum_\nu \sigma_i^{0\nu}(j, o; E_{ij})$, summed over all excited states of the final nucleus, with the target in

the ground state. Target states μ in an astrophysical plasma are thermally populated and the astrophysical cross section $\sigma_i^*(j, o)$ is given by

$$\sigma_i^*(j, o; E_{ij}) = \frac{\sum_{\mu} (2J_i^{\mu} + 1) \exp(-E_i^{\mu}/kT) \sum_{\nu} \sigma_i^{\mu\nu}(j, o; E_{ij})}{\sum_{\mu} (2J_i^{\mu} + 1) \exp(-E_i^{\mu}/kT)} . \quad (2.14)$$

The summation over ν replaces $T_o^{\nu}(E, J, \pi)$ in Eq.(2.13) by the total transmission coefficient

$$T_o(E, J, \pi) = \sum_{\nu=0}^{\nu_m} T_o^{\nu}(E, J, \pi, E_m^{\nu}, J_m^{\nu}, \pi_m^{\nu}) + \int_{E_m^{\nu_m}}^{E-S_{m,o}} \sum_{J_m, \pi_m} T_o(E, J, \pi, E_m, J_m, \pi_m) \rho(E_m, J_m, \pi_m) dE_m . \quad (2.15)$$

Here $S_{m,o}$ is the channel separation energy, and the summation over excited states above the highest experimentally known state ν_m is changed to an integration over the level density ρ . The summation over target states μ in Eq.(2.14) has to be generalized accordingly.

In addition to the ingredients required for Eq.(2.13), like the transmission coefficients for particles and photons, width fluctuation corrections $W(j, o, J, \pi)$ have to be employed. They define the correlation factors with which all partial channels for an incoming particle j and outgoing particle o , passing through the excited state (E, J, π) , have to be multiplied. This takes into account that the decay of the state is not fully statistical, but some memory of the way of formation is retained and influences the available decay choices. The major effect is elastic scattering, the incoming particle can be immediately re-emitted before the nucleus equilibrates. Once the particle is absorbed and not re-emitted in the very first (pre-compound) step, the equilibration is very likely. This corresponds to enhancing the elastic channel by a factor W_j . In order to conserve the total cross section, the individual transmission coefficients in the outgoing channels have to be renormalized to T_j' . The total cross section is proportional to T_j and, when summing over the elastic channel ($W_j T_j'$) and all outgoing channels ($T_{tot}' - T_j'$), one obtains the condition $T_j = T_j'(W_j T_j'/T_{tot}') + T_j'(T_{tot}' - T_j')/T_{tot}'$. We can (almost) solve for T_j'

$$T_j' = \frac{T_j}{1 + T_j'(W_j - 1)/T_{tot}'} . \quad (2.16)$$

This requires an iterative solution for T' (starting in the first iteration with T_j and T_{tot}), which converges fast. The enhancement factor W_j has to be known in order to apply Eq.(2.16). A general expression in closed form was derived by Verbaatschot et al. (1986), but is computationally expensive to use. A fit to results from Monte Carlo calculations by Tepel et al. (1974) gave

$$W_j = 1 + \frac{2}{1 + T_j^{1/2}} . \quad (2.17)$$

For a general discussion of approximation methods see Gadioli & Hodgson (1992) and Ezhov & Plujko (1993). Eqs.(2.16) and (2.17) redefine the transmission coefficients of Eq.(2.13) in such a manner that the total width is redistributed by enhancing the elastic channel and weak channels over the dominant one. Cross sections near threshold energies of new channel openings, where very different channel strengths exist, can only be described correctly when taking width fluctuation corrections into account. Of the thermonuclear rates presently available in the literature, only those by Thielemann et al. (1987)

and Cowan et al. (1991) included this effect, but their level density treatment still contained large uncertainties. The width fluctuation corrections of Tepel et al. (1974) are only an approximation to the correct treatment. However, Thomas et al. (1986) showed that they are quite adequate.

The important ingredients of statistical model calculations as indicated in Eqs.(2.13) through (2.15) are the particle and gamma-transmission coefficients T and the level density of excited states ρ . Therefore, the reliability of such calculations is determined by the accuracy with which these components can be evaluated (often for unstable nuclei). In the following we want to discuss the methods utilized to estimate these quantities and recent improvements.

2.2. Transmission Coefficients

The transition from an excited state in the compound nucleus (E, J, π) to the state $(E_i^\mu, J_i^\mu, \pi_i^\mu)$ in nucleus i via the emission of a particle j is given by a summation over all quantum mechanically allowed partial waves

$$T_j^\mu(E, J, \pi, E_i^\mu, J_i^\mu, \pi_i^\mu) = \sum_{l=|J-s|}^{J+s} \sum_{s=|J_i^\mu-J_j|}^{J_i^\mu+J_j} T_{jls}(E_{ij}^\mu). \quad (2.18)$$

Here the angular momentum \vec{l} and the channel spin $\vec{s} = \vec{J}_j + \vec{J}_i^\mu$ couple to $\vec{J} = \vec{l} + \vec{s}$. The transition energy in channel j is $E_{ij}^\mu = E - S_j - E_i^\mu$.

The individual particle transmission coefficients T_l are calculated by solving the Schrödinger equation with an optical potential for the particle-nucleus interaction. All early studies of thermonuclear reaction rates by Turan et al. (1966), Michaud & Fowler (1972), Arnould (1972), Turan (1972), Holmes et al. (1976), and Woosley et al. (1978) employed optical square well potentials and made use of the black nucleus approximation. Thielemann et al. (1987) employed the optical potential for neutrons and protons given by Jeukenne, Lejeune, & Mahaux (1977), based on microscopic infinite nuclear matter calculations for a given density, applied with a local density approximation. It includes corrections of the imaginary part by Fantoni et al. (1981) and Mahaux (1982). The resulting s-wave neutron strength function $\langle \Gamma^o/D \rangle_{1\text{eV}} = (1/2\pi)T_{n(l=0)}(1\text{eV})$ is shown and discussed in Thielemann et al. (1983) and Cowan et al. (1991), where several phenomenological optical potentials of the Woods-Saxon type and the equivalent square well potential used in earlier astrophysical applications are compared. The purely theoretical approach gives the best fit. It is also expected to have the most reliable extrapolation properties for unstable nuclei. We show here in Fig. 1 the ratio of the s-wave strength functions for the Jeukenne, Lejeune, & Mahaux potential over the black nucleus, equivalent square well approach for different energies. A general overview on different approaches can be found in Varner et al. (1991).

Deformed nuclei were treated in a very simplified way by using an effective spherical potential of equal volume, based on averaging the deformed potential over all possible angles between the incoming particle and the orientation of the deformed nucleus. In most earlier compilations alpha particles were also treated by square well optical potentials. Thielemann et al. (1987) employed a phenomenological Woods-Saxon potential by Mann (1978), based on extensive data from McFadden & Satchler (1966). For future use, for alpha particles and heavier projectiles, it is clear that the best results can probably be obtained with folding potentials [e.g. Satchler & Love (1979), Chaudhuri et al. (1985), Oberhummer et al. (1996), and Mohr et al. (1997)].

The gamma-transmission coefficients have to include the dominant gamma-transitions (E1 and M1) in the calculation of the total photon width. The smaller, and therefore

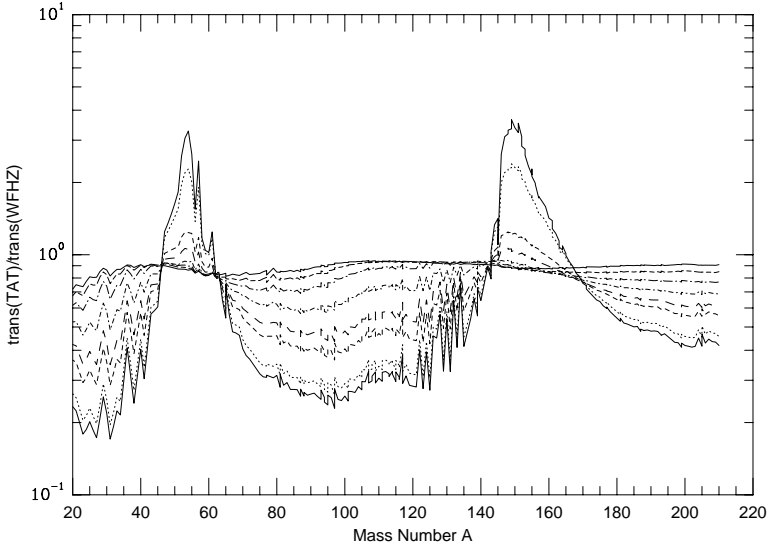


FIGURE 1. Ratios of transmission functions obtained with the Jeukenne et al. (1977) potential and the equivalent square well description of Woosley et al. (1978). Shown are the ratios for s-wave neutrons. Different line styles denote different energies: 0.01 MeV (solid), 0.1 MeV (dotted), 1.0 MeV (short dashes), 2.0 MeV (long dashes), 5.0 MeV (dot – short dash), 10.0 MeV (dot – long dash), 15.0 MeV (short dash – long dash), 20.0 MeV (solid).

less important, M1 transitions have usually been treated with the simple single particle approach $T \propto E^3$ of Blatt & Weisskopf (1952), as also discussed in Holmes et al. (1976). The E1 transitions are usually calculated on the basis of the Lorentzian representation of the Giant Dipole Resonance (GDR). Within this model, the E1 transmission coefficient for the transition emitting a photon of energy E_γ in a nucleus ${}^A_Z X$ is given by

$$T_{E1}(E_\gamma) = \frac{8}{3} \frac{NZ}{A} \frac{e^2}{\hbar c} \frac{1 + \chi}{mc^2} \sum_{i=1}^2 \frac{i}{3} \frac{\Gamma_{G,i} E_\gamma^4}{(E_\gamma^2 - E_{G,i}^2)^2 + \Gamma_{G,i}^2 E_\gamma^2} . \quad (2.19)$$

Here $\chi (= 0.2)$ accounts for the neutron-proton exchange contribution as discussed in Lipparini & Stringari (1989), and the summation over i includes two terms which correspond to the split of the GDR in statically deformed nuclei, with oscillations along ($i=1$) and perpendicular ($i=2$) to the axis of rotational symmetry. Many microscopic and macroscopic models have been devoted to the calculation of the GDR energies (E_G) and widths (Γ_G). Analytical fits as a function of A and Z were also used, e.g. in Holmes et al. (1976) and Woosley et al. (1978). Thielemann et al. (1987) employed the (hydrodynamic) droplet model approach by Myers et al. (1977) for E_G , which gives an excellent fit to the GDR energies and can also predict the split of the resonance for deformed nuclei, when making use of the deformation, calculated within the droplet model. In that case, the two resonance energies are related to the mean value calculated by the relations $E_{G,1} + 2E_{G,2} = 3E_G$, $E_{G,2}/E_{G,1} = 0.911\eta + 0.089$ of Danos (1958). η is the ratio of the diameter along the nuclear symmetry axis to the diameter perpendicular

to it, and can be obtained from the experimentally known deformation or mass model predictions.

Cowan et al. (1991) also give a detailed description of the microscopic-macroscopic approach utilized to calculate Γ_G , based on dissipation and the coupling to quadrupole surface vibrations. This is the method applied to predict the gamma-transmission coefficients for the cross section determinations shown in the following.

2.3. Level Densities

While the method as such is well seasoned, considerable effort has been put into the improvement of the input for statistical Hauser-Feshbach models. However, the nuclear level density has given rise to the largest uncertainties in cross section determinations of Holmes et al. (1976), Thielemann et al. (1987), Thielemann et al. (1988), and Cowan et al. (1991). For large scale astrophysical applications it is also necessary to not only find reliable methods for level density predictions, but also computationally feasible ones.

Such a model is the non-interacting Fermi-gas model by Bethe (1936). Most statistical model calculations use the back-shifted Fermi-gas description of Gilbert & Cameron (1965). More sophisticated Monte Carlo shell model calculations, e.g. by Dean et al. (1995), as well as combinatorial approaches [see e.g. Paar (1997)], have shown excellent agreement with this phenomenological approach and justified the application of the Fermi-gas description at and above the neutron separation energy. Rauscher, Thielemann, & Kratz (1997) applied an energy-dependent level density parameter a together with microscopic corrections from nuclear mass models, which leads to improved fits in the mass range $20 \leq A \leq 245$.

The back-shifted Fermi-gas description of Gilbert & Cameron (1965) assumes an even distribution of odd and even parities [however, see e.g. Pichon (1994) for doubts on the validity of this assumption at energies of astrophysical interest]

$$\rho(U, J, \pi) = \frac{1}{2} \mathcal{F}(U, J) \rho(U), \quad (2.20)$$

with

$$\rho(U) = \frac{1}{\sqrt{2\pi\sigma}} \frac{\sqrt{\pi}}{12a^{1/4}} \frac{\exp(2\sqrt{aU})}{U^{5/4}}, \quad \mathcal{F}(U, J) = \frac{2J+1}{2\sigma^2} \exp\left(\frac{-J(J+1)}{2\sigma^2}\right) \quad (2.21)$$

$$\sigma^2 = \frac{\Theta_{\text{rigid}}}{\hbar^2} \sqrt{\frac{U}{a}}, \quad \Theta_{\text{rigid}} = \frac{2}{5} m_{\text{n}} AR^2, \quad U = E - \delta \quad .$$

The spin dependence \mathcal{F} is determined by the spin cut-off parameter σ . Thus, the level density is dependent on only two parameters: the level density parameter a and the backshift δ , which determines the energy of the first excited state.

Within this framework, the quality of level density predictions depends on the reliability of systematic estimates of a and δ . The first compilation for a large number of nuclei was provided by Gilbert & Cameron (1965). They found that the backshift δ is well reproduced by experimental pairing corrections (Cameron & Elkin 1965). They also were the first to identify an empirical correlation with experimental shell corrections $S(Z, N)$

$$\frac{a}{A} = c_0 + c_1 S(Z, N), \quad (2.22)$$

where $S(Z, N)$ is negative near closed shells. The back-shifted Fermi-gas approach diverges for $U = 0$ (i.e. $E = \delta$, if δ is a positive backshift). In order to obtain the correct behavior at very low excitation energies, the Fermi-gas description can be combined with the

constant temperature formula [Gilbert & Cameron (1965), Gadioli & Hodgson (1992) and references therein]

$$\rho(U) \propto \frac{\exp(U/T)}{T} . \quad (2.23)$$

The two formulations are matched by a tangential fit determining T . There have been a number of compilations for a and δ , or T , based on experimental level densities, as e.g. the ones by von Egidy *et al.* (1986,1988). An improved approach has to consider the energy dependence of the shell effects, which are known to vanish at high excitation energies, see e.g. Iljinov *et al.* (1992). Although, for astrophysical purposes only energies close to the particle separation thresholds have to be considered, an energy dependence can lead to a considerable improvement of the global fit. This is especially true for strongly bound nuclei close to magic numbers.

An excitation-energy dependent description was initially proposed by Ignatyuk *et al.* (1975) and Ignatyuk *et al.* (1979) for the level density parameter a

$$a(U, Z, N) = \tilde{a}(A) \left[1 + C(Z, N) \frac{f(U)}{U} \right] \quad (2.24a)$$

$$\tilde{a}(A) = \alpha A + \beta A^{2/3} \quad (2.24b)$$

$$f(U) = 1 - \exp(-\gamma U). \quad (2.24c)$$

The values of the free parameters α , β and γ are determined by fitting to experimental level density data available over the whole nuclear chart.

The shape of the function $f(U)$ permits the two extremes: (i) for small excitation energies the original form of Eq.(2.22) $a/A = \alpha + \alpha\gamma C(Z, N)$ is retained with $S(Z, N)$ being replaced by $C(Z, N)$, (ii) for high excitation energies a/A approaches the continuum value α , obtained for infinite nuclear matter. In both cases we neglected β , which is realistic as discussed below. Previous attempts to find a global description of level densities used shell corrections S derived from comparison of liquid-drop masses with experiment ($S \equiv M_{\text{exp}} - M_{\text{LD}}$) or the “empirical” shell corrections $S(Z, N)$ given by Gilbert & Cameron (1965). A problem connected with the use of liquid-drop masses arises from the fact that there are different liquid-drop model parametrizations available in the literature which produce quite different values for S , as shown in Mengoni & Nakayama (1994).

However, in addition, the meaning of the correction parameter inserted into the level density formula Eq.(2.24) has to be reconsidered. The fact that nuclei approach a spherical shape at high excitation energies (temperatures) has to be included. Therefore, the correction parameter C should describe properties of a nucleus differing from the *spherical* macroscopic energy and contain those terms which are finite for low and vanishing at higher excitation energies. The latter requirement is mimicked by the form of Eq.(2.24). Therefore, the parameter $C(Z, N)$ should rather be identified with the so-called “microscopic” correction E_{mic} than with the shell correction. The mass of a nucleus with deformation ϵ can then be written in two ways

$$M(\epsilon) = E_{\text{mic}}(\epsilon) + E_{\text{mac}}(\text{spherical}) \quad (2.25a)$$

$$M(\epsilon) = E_{\text{mac}}(\epsilon) + E_{\text{s+p}}(\epsilon), \quad (2.25b)$$

with $E_{\text{s+p}}$ being the shell-plus-pairing correction. This confusion about the term “microscopic correction”, being sometimes used in an ambiguous way, is also pointed out in Möller *et al.* (1995). The above mentioned ambiguity follows from the inclusion of deformation-dependent effects into the macroscopic part of the mass formula.

Another important ingredient is the pairing gap Δ , related to the backshift δ . Instead

of assuming constant pairing as in Reisdorf (1981) or an often applied fixed dependence on the mass number via e.g. $\pm 12/\sqrt{A}$, the pairing gap Δ can be determined from differences in the binding energies (or mass differences, respectively) of neighboring nuclei. Thus, similar to Ring & Schuck (1980), Wang et al. (1992) obtained for the neutron pairing gap Δ_n

$$\Delta_n(Z, N) = \frac{1}{2} [M(Z, N-1) + M(Z, N+1) - 2M(Z, N)], \quad (2.26)$$

where $M(Z, N)$ is the ground state mass excess of the nucleus (Z, N) . Similarly, the proton pairing gap Δ_p can be calculated.

2.4. Results

In our study we utilized the microscopic corrections of the recent mass formula by Möller et al. (1995), calculated with the Finite Range Droplet Model FRDM (using a folded Yukawa shell model with Lipkin-Nogami pairing) in order to determine the parameter $C(Z, N) = E_{\text{mic}}$. The backshift δ was calculated by setting $\delta(Z, N) = 1/2 \{ \Delta_n(Z, N) + \Delta_p(Z, N) \}$ and using Eq.(2.26). The parameters α , β , and γ were obtained from a fit to experimental data for s-wave neutron resonance spacings of 272 nuclei at the neutron separation energy. The data were taken from the compilation by Iljinov et al. (1992). Similar investigations were recently undertaken by Mengoni & Nakajima (1994), who made, however, use of a slightly different description of the energy dependence of a and of different pairing gaps.

As a quantitative overall estimate of the agreement between calculations and experiments, one usually quotes the ratio

$$g \equiv \left\langle \frac{\rho_{\text{calc}}}{\rho_{\text{exp}}} \right\rangle = \exp \left[\frac{1}{n} \sum_{i=1}^n \left(\ln \frac{\rho_{\text{calc}}^i}{\rho_{\text{exp}}^i} \right)^2 \right]^{1/2}, \quad (2.27)$$

with n being the number of nuclei for which level densities ρ are experimentally known. As best fit we obtain an averaged ratio $g = 1.48$ with the parameter values $\alpha = 0.1337$, $\beta = -0.06571$, $\gamma = 0.04884$. This corresponds to $a/A = \alpha = 0.134$ for infinite nuclear matter, which is approached for high excitation energies. The ratios of experimental to predicted level densities (i.e. theoretical to experimental level spacings D) for the nuclei considered are shown in Fig. 2. As can be seen, for the majority of nuclei the absolute deviation is less than a factor of 2. This is a satisfactory improvement over theoretical level densities used in previous astrophysical cross section calculations, where deviations of a factor 3–4, or even in excess of a factor of 10 were found [for details see Cowan et al. (1991)]. Such a direct comparison as in Fig. 2 was rarely shown in earlier work. In most cases the level density parameter a , entering exponentially into the level density, was displayed.

Although we quoted the value of the parameter β above, it is small in comparison to α and can be set to zero without considerable increase in the obtained deviation. Therefore, actually only two parameters are needed for the level density description. Rauscher, Thielemann, & Kratz (1997) also tested the sensitivity with respect to the employed mass formula. This phenomenological approach, still in the framework of the back-shifted Fermi gas model, but with an energy dependent level density parameter, based on microscopic corrections of nuclear mass models, gives better results than a recent BCS approach by Goriely (1996), which tried to implement level spacings from the ETFSI model (Extended Thomas-Fermi with Strutinski Integral, Aboussir et al. 1995) in a consistent combinatorial fashion.

With these improvements, the uncertainty in the level density is now comparable to

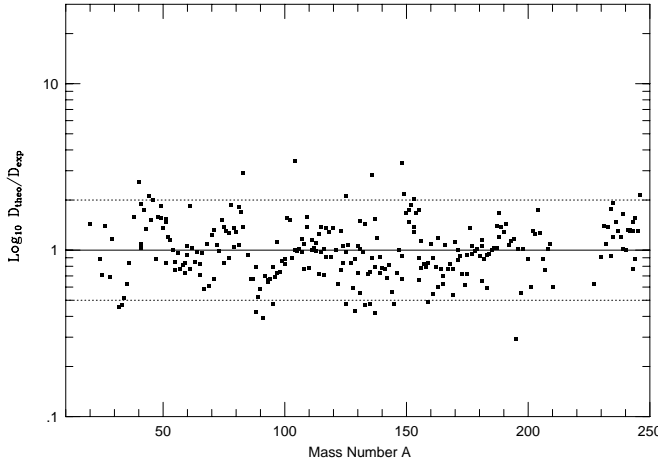


FIGURE 2. Ratio of predicted to experimental Iljinov et al. (1992) level densities at the neutron separation energy. The deviation is less than a factor of 2 (dotted lines) for the majority of the considered nuclei.

uncertainties in optical potentials and gamma transmission coefficients which enter the determinations of capture cross sections. The remaining uncertainty of extrapolations is the one due to the reliability of the nuclear structure model applied far from stability which provides the microscopic corrections and pairing gaps. We will discuss this in more detail in section 5 (see also the contribution by M. Wiescher, this volume).

2.5. *Applicability of the Statistical Model*

Having a reliable level density description also permits to analyze when and where the statistical model approach is valid. Generally speaking, in order to apply the model correctly, a sufficiently large number of levels in the compound nucleus is needed in the relevant energy range, which can act as doorway states to the formation of the compound nucleus. In the following this is discussed for neutron-, proton- and alpha-induced reactions with the aid of the level density approach presented above. This section is intended to be a guide to a meaningful and correct application of the statistical model.

The nuclear reaction rate per particle pair at a given stellar temperature T is determined by folding the reaction cross section with the Maxwell-Boltzmann (MB) velocity distribution of the projectiles, as displayed in Eq.(1.4). Two cases have to be considered, reactions between charged particles and reactions with neutrons.

2.5.1. *The Effective Energy Window*

The nuclear cross section for charged particles is strongly suppressed at low energies due to the Coulomb barrier. For particles having energies less than the height of the Coulomb barrier, the product of the penetration factor and the MB distribution function at a given temperature results in the so-called Gamow peak, in which most of the reactions will take place. Location and width of the Gamow peak depend on the charges of projectile and target, and on the temperature of the interacting plasma.

When introducing the astrophysical S factor $S(E) = \sigma(E)E \exp(2\pi\eta)$ (with η being the Sommerfeld parameter, describing the s-wave barrier penetration), one can easily see

the two contributions of the velocity distribution and the penetrability in the integral

$$\langle \sigma v \rangle = \left(\frac{8}{\pi\mu} \right)^{1/2} \frac{1}{(kT)^{3/2}} \int_0^\infty S(E) \exp \left[-\frac{E}{kT} - \frac{b}{E^{1/2}} \right] , \quad (2.28)$$

where the quantity $b = 2\pi\eta E^{1/2} = (2\mu)^{1/2} \pi e^2 Z_j Z_k / \hbar$ arises from the barrier penetrability. Taking the first derivative of the integrand yields the location E_0 of the Gamov peak, and the effective width Δ of the energy window can be derived accordingly

$$E_0 = \left(\frac{bkT}{2} \right)^{2/3} = 1.22 (Z_j^2 Z_k^2 AT_6^2)^{1/3} \text{ keV}, \quad (2.29a)$$

$$\Delta = \frac{16E_0 kT^{1/2}}{3} = 0.749 (Z_j^2 Z_k^2 AT_6^5)^{1/6} \text{ keV}, \quad (2.29b)$$

as shown in Fowler et al. (1967) and Rolfs & Rodney (1988), where the charges Z_j , Z_k , the reduced mass A of the involved nuclei in units of m_u , and the temperature T_6 given in 10^6 K, enter.

In the case of neutron-induced reactions the effective energy window has to be derived in a slightly different way. For s-wave neutrons ($l = 0$) the energy window is simply given by the location and width of the peak of the MB distribution function. For higher partial waves the penetrability of the centrifugal barrier shifts the effective energy E_0 to higher energies. For neutrons with energies less than the height of the centrifugal barrier this was approximated by Wagoner (1969)

$$E_0 \approx 0.172T_9 \left(l + \frac{1}{2} \right) \text{ MeV}, \quad (2.30a)$$

$$\Delta \approx 0.194T_9 \left(l + \frac{1}{2} \right)^{1/2} \text{ MeV}. \quad (2.30b)$$

The energy E_0 will always be comparatively close to the neutron separation energy.

2.5.2. A Criterion for the Application of the Statistical Model

Using the above effective energy windows for charged and neutral particle reactions, a criterion for the applicability can be derived from the level density. For a reliable application of the statistical model a sufficient number of nuclear levels has to be within the energy window, thus contributing to the reaction rate. For narrow, isolated resonances, the cross sections (and also the reaction rates) can be represented by a sum over individual Breit-Wigner terms. The main question is whether the density of resonances (i.e. level density) is high enough so that the integral over the sum of Breit-Wigner resonances may be approximated by an integral over the statistical model expressions of Eq.(2.13), which assume that at any bombarding energy a resonance of any spin and parity is available [see Wagoner (1969)].

Numerical test calculations have been performed by Rauscher et al. (1997) in order to find the average number of levels per energy window which is sufficient to allow this substitution in the specific case of folding over a MB distribution. To achieve 20% accuracy, about 10 levels in total are needed in the effective energy window in the worst case (non-overlapping, narrow resonances). This relates to a number of s-wave levels smaller than 3. Application of the statistical model for a level density which is not sufficiently large, results in general in an overestimation of the actual cross section, unless a strong s-wave resonance is located right in the energy window [see the discussion in van Wormer et al. (1994)]. Therefore, we will assume in the following a conservative

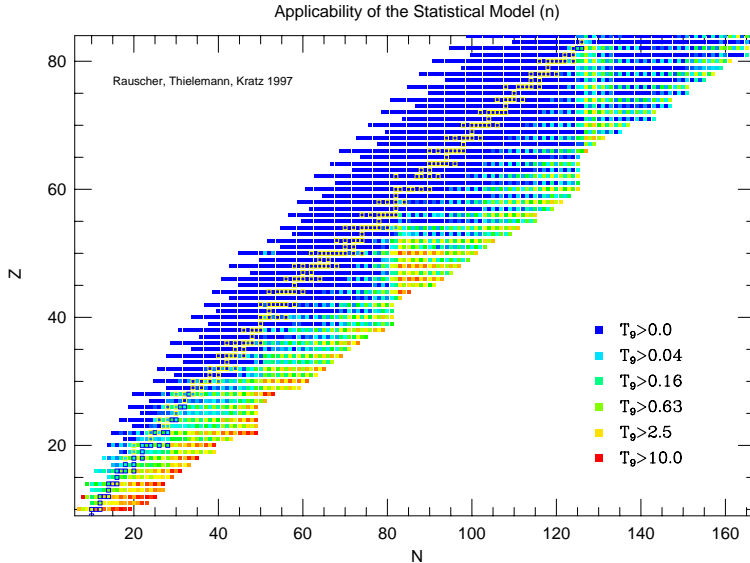


FIGURE 3. Stellar temperatures (in 10^9 K) for which the statistical model can be used. Plotted is the compound nucleus of the neutron-induced reaction $n+\text{Target}$. Stable nuclei are marked.

limit of 10 contributing resonances in the effective energy window for charged and neutral particle-induced reactions.

To obtain the necessary number of levels within the energy window of width Δ can require a sufficiently high excitation energy, as the level density increases with energy. This combines with the thermal distribution of projectiles to a minimum temperature for the application of the statistical model. Those temperatures are plotted in a logarithmic grey scale in Figs. 3–5. For neutron-induced reactions Fig. 3 applies, Fig. 4 describes proton-induced reactions, and Fig. 5 alpha-induced reactions. Plotted is always the minimum stellar temperature T_9 (in 10^9 K) at the location of the compound nucleus in the nuclear chart. It should be noted that the derived temperatures will not change considerably, even when changing the required level number within a factor of about two, because of the exponential dependence of the level density on the excitation energy.

This permits to read directly from the plot whether the statistical model cross section can be “trusted” for a specific astrophysical application at a specified temperature or whether single resonances or other processes (e.g. direct reactions) have also to be considered. These plots can give hints on when it is safe to use the statistical model approach and which nuclei have to be treated with special attention for specific temperatures. Thus, information on which nuclei might be of special interest for an experimental investigation may also be extracted.

3. Nucleosynthesis Processes in Stellar Evolution and Explosions

Nucleosynthesis calculations can in general be classified into two categories: (1) nucleosynthesis during hydrostatic burning stages of stellar evolution on long timescales and (2) nucleosynthesis in explosive events (with different initial fuel compositions, specific

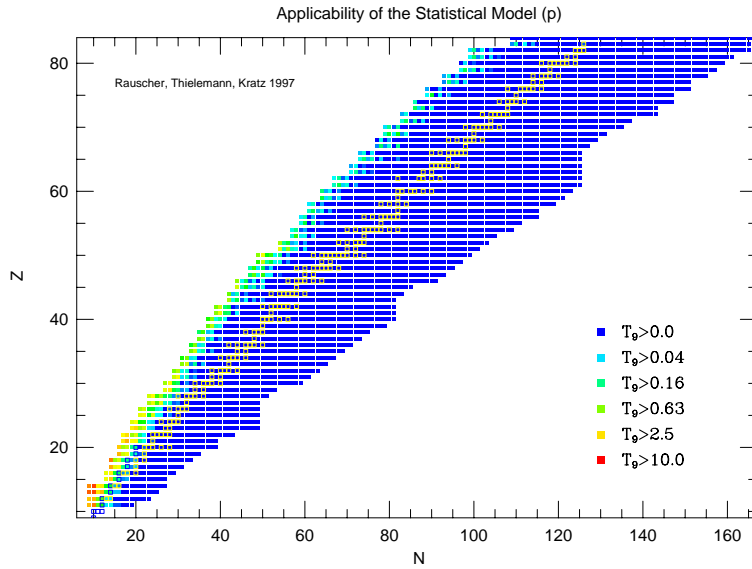


FIGURE 4. Stellar temperatures (in 10^9) for which the statistical model can be used. Plotted is the compound nucleus of the proton-induced reaction $p+\text{Target}$. Stable nuclei are marked.

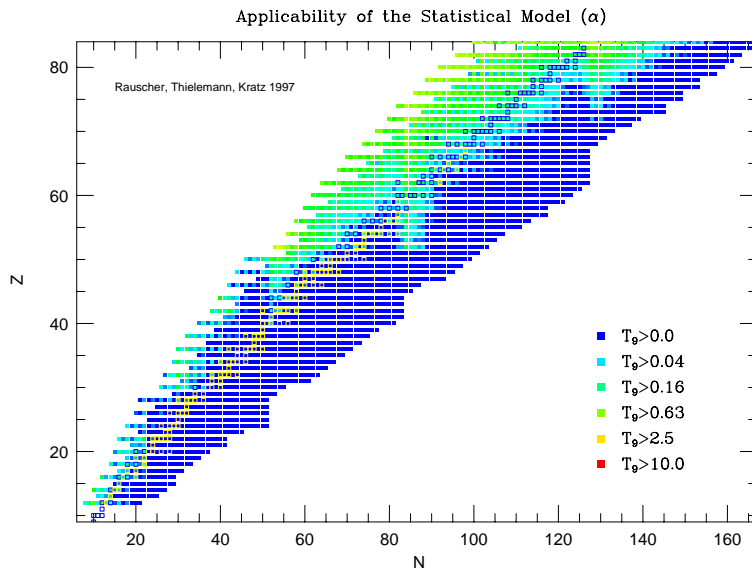


FIGURE 5. Stellar temperatures (in 10^9) for which the statistical model can be used. Plotted is the compound nucleus of the alpha-induced reaction $\alpha+\text{Target}$. Stable nuclei are marked.

to the event). In the following we want to discuss shortly reactions of importance for both conditions and the major burning products.

3.1. *Hydrostatic Burning Stages in Presupernova Evolution*

The main hydrostatic burning stages and most important reactions are:

H-burning: there are two alternative reaction sequences, the different pp-chains which convert ${}^1\text{H}$ into ${}^4\text{He}$, initiated by ${}^1\text{H}(p, e^+){}^2\text{H}$, and the CNO cycle which converts ${}^1\text{H}$ into ${}^4\text{He}$ by a sequence of (p, γ) and (p, α) reactions on C, N, and O isotopes and subsequent beta-decays. The CNO isotopes are all transformed into ${}^{14}\text{N}$, due to the fact that the reaction ${}^{14}\text{N}(p, \gamma){}^{15}\text{O}$ is the slowest reaction in the cycle.

He-burning: the main reactions are the triple-alpha reaction ${}^4\text{He}(2\alpha, \gamma){}^{12}\text{C}$ and ${}^{12}\text{C}(\alpha, \gamma){}^{16}\text{O}$.

C-burning: ${}^{12}\text{C}({}^{12}\text{C}, \alpha){}^{20}\text{Ne}$ and ${}^{12}\text{C}({}^{12}\text{C}, p){}^{23}\text{Na}$. Most of the ${}^{23}\text{Na}$ nuclei will react with the free protons via ${}^{23}\text{Na}(p, \alpha){}^{20}\text{Ne}$.

Ne-Burning: ${}^{20}\text{Ne}(\gamma, \alpha){}^{16}\text{O}$, ${}^{20}\text{Ne}(\alpha, \gamma){}^{24}\text{Mg}$ and ${}^{24}\text{Mg}(\alpha, \gamma){}^{28}\text{Si}$. It is important that photodisintegrations start to play a role when $30kT \approx Q$ (as a rule of thumb), with Q being the Q-value of a capture reaction. For those conditions sufficient photons with energies $>Q$ exist in the high energy tail of the Planck distribution. As ${}^{16}\text{O}(\alpha, \gamma){}^{20}\text{Ne}$ has an exceptionally small Q-value of the order 4 MeV, this relation holds true for $T > 1.5 \times 10^9\text{K}$, which is the temperature for (hydrostatic) Ne-burning.

O-burning: ${}^{16}\text{O}({}^{16}\text{O}, \alpha){}^{28}\text{Si}$, ${}^{16}\text{O}({}^{16}\text{O}, p){}^{31}\text{P}$, and ${}^{16}\text{O}({}^{16}\text{O}, n){}^{31}\text{S}(\beta^+){}^{31}\text{P}$. Similar to carbon burning, most of the ${}^{31}\text{P}$ is destroyed by a (p, α) reaction to ${}^{28}\text{Si}$.

Si-burning: Si-burning is initiated like Ne-burning by photodisintegration reactions which then provide the particles for capture reactions. It ends in an equilibrium abundance distribution around Fe (thermodynamic equilibrium). As this includes all kinds of Q-values (on the average 8-10 MeV for capture reactions along the valley of stability), this translates to temperatures in excess of $3 \times 10^9\text{K}$, being larger than the temperatures for the onset of Ne-burning. In such an equilibrium (also denoted nuclear statistical equilibrium, NSE) the abundance of each nucleus is only governed by the temperature T , density ρ , its nuclear binding energy B_i and partition function $G_i = \sum_j (2J_j^i + 1) \exp(-E_j^i/kT)$

$$Y_i = (\rho N_A)^{A_i-1} \frac{G_i}{2^{A_i}} A_i^{3/2} \left(\frac{2\pi\hbar^2}{m_u kT} \right)^{\frac{3}{2}(A_i-1)} \exp(B_i/kT) Y_p^{Z_i} Y_n^{N_i}, \quad (3.31)$$

while fulfilling mass conservation $\sum_i A_i Y_i = 1$ and charge conservation $\sum_i Z_i Y_i = Y_e$ (the total number of protons equals the net number of electrons, which is usually changed only by weak interactions on longer timescales). This equation is derived from the relation between chemical potentials (for Maxwell-Boltzmann distributions) in a thermal equilibrium ($\mu_i = Z_i \mu_p + N_i \mu_n$), where the subscripts n and p stand for neutrons and protons. Intermediate quasi-equilibrium stages (QSE), where clusters of neighboring nuclei are in relative equilibrium via neutron and proton reactions, but different clusters have total abundances which are offset from their NSE values, are important during the onset of Si-burning before a full NSE is reached and during the freeze-out from high temperatures, which will be discussed in section 3.2.

s-process: the slow neutron capture process leads to the build-up of heavy elements during core and shell He-burning, where through a series of neutron captures and beta-decays, starting on existing heavy nuclei around Fe, nuclei up to Pb and Bi can be synthesized. The neutrons are provided by a side branch of He-burning, ${}^{14}\text{N}(\alpha, \gamma){}^{18}\text{F}(\beta^+){}^{18}\text{O}(\alpha, \gamma){}^{22}\text{Ne}(\alpha, n){}^{25}\text{Mg}$. An alternative stronger neutron source in He-shell flashes is the reaction

$^{13}\text{C}(\alpha, n)^{16}\text{O}$, which requires admixture of hydrogen and the production of ^{13}C via proton capture on ^{12}C and a subsequent beta-decay.

An extensive overview over the major and minor reaction sequences in all burning stages from helium to silicon burning in massive stars is given in Arnett & Thielemann (1985), Thielemann & Arnett (1985), Woosley & Weaver (1995), Hix & Thielemann (1996) and Nomoto et al. (1997) (see also Arnett 1996 and for the status of experimental rate uncertainties M. Wiescher, this volume). For less massive stars which burn at higher densities, i.e. experience higher electron Fermi energies, electron captures are already important in O-burning and lead to a smaller Y_e or larger neutron excess $\eta = \sum_i (N_i - Z_i) Y_i = 1 - 2Y_e$. For a general overview of the s-process see Käppeler, Beer, & Wisshak (1989), Käppeler et al. (1994), Wisshak et al. (1997), and Gallino & Busso (1997).

Most reactions in hydrostatic burning stages proceed through stable nuclei. This is simply explained by the long timescales involved. For a $25M_\odot$ star, which is relatively massive and therefore experiences quite short burning phases, this still amounts to: H-burning 7×10^6 years, He-burning 5×10^5 y, C-burning 600 y, Ne-burning 1 y, O-burning 180 days, Si-burning 1 d. Because all these burning stages are long compared to beta-decay half-lives, with a few exceptions of long-lived unstable nuclei, nuclei can decay back to stability before undergoing the next reaction. Examples of such exceptions are the s-process branchings with a competition between neutron captures and beta-decays of similar timescales (see e.g. Gallino & Busso 1997).

3.2. Explosive Burning

Many of the hydrostatic burning processes discussed in section 3.1 can occur also under explosive conditions at much higher temperatures and on shorter timescales. The major reactions remain still the same in many cases, but often the beta-decay half-lives of unstable products are longer than the timescales of the explosive processes under investigation. This requires in general the additional knowledge of nuclear cross sections for unstable nuclei.

Extensive calculations of explosive carbon, neon, oxygen, and silicon burning, appropriate for supernova explosions, have already been performed in the late 60s and early 70s with the accuracies possible in those days and detailed discussions about the expected abundance patterns (for a general review see Trimble 1975; Truran 1985). More recent overviews in the context of stellar models are given by Trimble (1991) and Arnett (1995). Besides minor additions of ^{22}Ne after He-burning (or nuclei which originate from it in later burning stages, see section 3.1), the fuels for explosive nucleosynthesis consist mainly of alpha-particle nuclei like ^{12}C , ^{16}O , ^{20}Ne , ^{24}Mg , or ^{28}Si . Because the timescale of explosive processing is very short (a fraction of a second to several seconds), only few beta-decays can occur during explosive nucleosynthesis events, resulting in heavier nuclei, again with $N \approx Z$. However, a spread of nuclei around a line of $N=Z$ is involved and many reaction rates for unstable nuclei have to be known. Dependent on the temperature, explosive burning produces intermediate to heavy nuclei. We will discuss the individual burning processes below. For the processes discussed in this section, nuclei within a few mass units from stability are encountered, where nuclear masses and decay half-lives are known experimentally.

Two processes differ from the above scenario, where either a large supply of neutrons or protons is available, the r-process and the rp-process, denoting rapid neutron or proton capture (the latter also termed explosive hydrogen burning). In such cases, nuclei close to the neutron and proton drip lines can be produced and beta-decay timescales can be

short in comparison to the process timescales. In this section we will only discuss the possible connection between explosive Si-burning and the r-process.

Burning timescales in stellar evolution are dictated by the energy loss timescales of stellar environments. Processes like hydrogen and helium burning, where the stellar energy loss is dominated by the photon luminosity, choose temperatures with energy generation rates equal to the radiation losses. For the later burning stages neutrino losses play the dominant role among cooling processes and the burning timescales are determined by temperatures where neutrino losses are equal to the energy generation rate (see the long series of investigations by Itoh and collaborators, e.g. Itoh et al. 1993, 1994, 1996ab). Explosive events are determined by hydrodynamics, causing different temperatures and timescales for the burning of available fuel. We can generalize the question by defining a burning timescale according to Eq.(1.11) for the destruction of the major fuel nuclei i

$$\tau_i = \left| \frac{Y_i}{\dot{Y}_i} \right|. \quad (3.32)$$

These timescales for the fuels $i \in \text{H, He, C, Ne, O, Si}$ are determined by the major destruction reaction. They are in all cases temperature dependent. Dependent on whether this is (i) a decay or photodisintegration, (ii) a two-particle or (iii) a three-particle fusion reaction, they are (i) either not density dependent or have an inverse (ii) linear or (iii) quadratic density dependence. Thus, in the burning stages which involve a fusion process, the density dependence is linear, with the exception of He-burning, where it is quadratic. Ne- and Si-burning, which are dominated by (γ, α) destructions of ^{20}Ne and ^{28}Si , have timescales only determined by the burning temperatures. The temperature dependences are typically exponential, due to the functional form of the corresponding $N_A \langle \sigma v \rangle$ expressions. We have plotted these burning timescales as a function of temperature (see Figs. 6 and 7), assuming a fuel mass fraction of 1. The curves for (also) density dependent burning processes are labeled with a typical density. He-burning has a quadratic density dependence, C- and O-burning depend linearly on density. If we take typical explosive burning timescales to be of the order of seconds (e.g. in supernovae), we see that one requires temperatures to burn essential parts of the fuel in excess of $4 \times 10^9 \text{K}$ (Si-burning), $3.3 \times 10^9 \text{K}$ (O-burning), $2.1 \times 10^9 \text{K}$ (Ne-burning), and $1.9 \times 10^9 \text{K}$ (C-burning). Beyond 10^9K He-burning is determined by an almost constant burning timescale. We see that essential destruction on a time scale of 1s is only possible for densities $\rho > 10^5 \text{g cm}^{-3}$. This is usually not encountered in He-shells of massive stars. In a similar way explosive H-burning is not of relevance for massive stars, but important for explosive burning in accreted H-envelopes in binary stellar evolution (these issues are discussed by M. Wiescher, this volume).

3.2.1. Explosive He-Burning

Explosive He-burning is characterized by the same reactions as hydrostatic He-burning, producing ^{12}C and ^{16}O . Fig. 6 indicated that even for temperatures beyond 10^9K high densities ($> 10^5 \text{g cm}^{-3}$) are required to burn essential amounts of He. During the passage of a 10^{51}erg supernova shockfront through the He-burning zones of a $25 M_\odot$ star, maximum temperatures of only $(6-9) \times 10^8 \text{K}$ are attained and the amount of He burned is negligible. However, neutron sources like $^{22}\text{Ne}(\alpha, n)^{25}\text{Mg}$ [or $^{13}\text{C}(\alpha, n)^{16}\text{O}$], which sustain an s-process neutron flux in hydrostatic burning, release a large neutron flux under explosive conditions. This leads to partial destruction of ^{22}Ne and the build-up of $^{25,26}\text{Mg}$ via $^{22}\text{Ne}(\alpha, n)^{25}\text{Mg}(n, \gamma)^{26}\text{Mg}$. Similarly, ^{18}O and ^{13}C are destroyed by alpha-induced reactions. This releases neutrons with $Y_n \approx 2 \times 10^{-9}$ at a density of $\approx 8.3 \times 10^3 \text{g}$

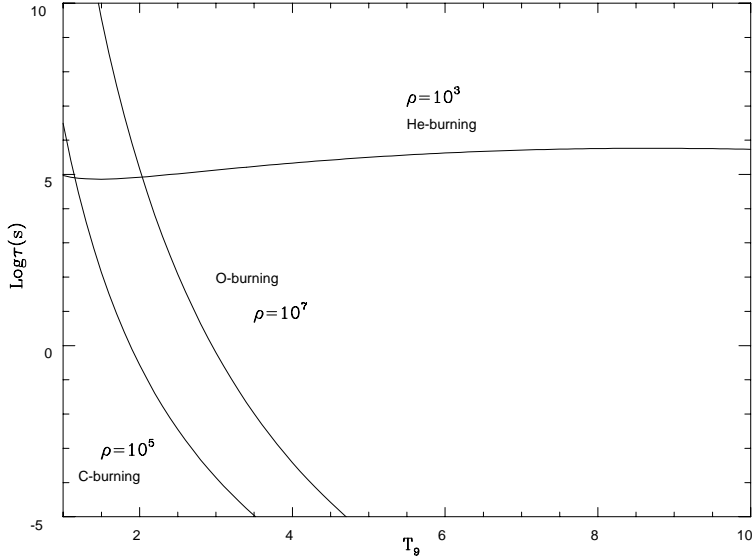


FIGURE 6. Burning timescales for fuel destruction of He-, C-, and O-burning as a function of temperature. A 100% fuel mass fraction was assumed. The factor $N_{i,i}^i = N_i/N_i!$ cancels for the destruction of identical particles by fusion reactions, as $N_i=2$. For He-burning the destruction of three identical particles has to be considered, which changes the leading factor $N_{i,i,i}^i$ to $1/2$. The density-dependent burning timescales are labeled with the chosen typical density. They scale linearly for C- and O-burning and quadratically for He-burning. Notice that the almost constant He-burning timescale beyond $T_9=1$ has the effect that efficient destruction on explosive timescales can only be attained for high densities.

cm^{-3} , corresponding to $n_n \approx 10^{19} \text{cm}^{-3}$ for about 0.2s, and causes neutron processing (Truran, Cowan, & Cameron 1978, Thielemann, Arnould, & Hillebrandt 1979, Thielemann, Metzinger, & Klapdor 1983, Cowan, Cameron, & Truran 1983). This is, however, not an r-process (Blake et al. 1981). More detailed calculations for such mass zones have recently been performed by Howard, Meyer, & Clayton (1992).

3.2.2. Explosive C- and Ne-Burning

The main burning products of explosive neon burning are ^{16}O , ^{24}Mg , and ^{28}Si , synthesized via the reaction sequences $^{20}\text{Ne}(\gamma, \alpha)^{16}\text{O}$ and $^{20}\text{Ne}(\alpha, \gamma)^{24}\text{Mg}(\alpha, \gamma)^{28}\text{Si}$, similar to the hydrostatic case. The mass zones in supernovae which undergo explosive neon burning must have peak temperatures in excess of $2.1 \times 10^9 \text{K}$. They undergo a combined version of explosive neon and carbon burning (see Figs. 6 and 7). Mass zones which experience temperatures in excess of $1.9 \times 10^9 \text{K}$ will undergo explosive carbon burning, as long as carbon fuel is available. This is often not the case in type II supernovae originating from massive stars. Besides the major abundances, mentioned above, explosive neon burning supplies also substantial amounts of ^{27}Al , ^{29}Si , ^{32}S , ^{30}Si , and ^{31}P . Explosive carbon burning contributes in addition the nuclei ^{20}Ne , ^{23}Na , ^{24}Mg , ^{25}Mg , and ^{26}Mg . Many nuclei in the mass range $20 < A < 30$ can be reproduced in solar proportions. This was confirmed for realistic stellar conditions by Morgan (1980). As photodisintegrations become important in explosive Ne-burning, also heavier pre-existing nuclei in such burning shells, from previous s- or r-processing (originating from prior stellar evolution or earlier stellar generations), can undergo e.g. (γ, n) or (γ, α) reactions. These can pro-

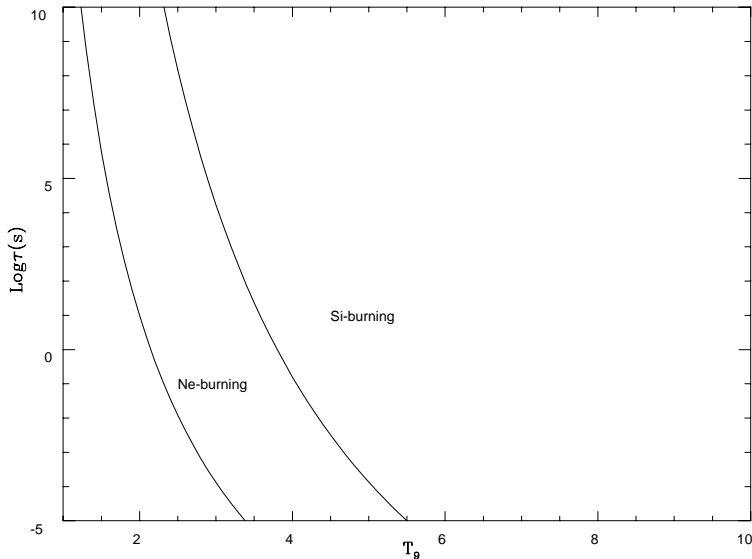


FIGURE 7. Burning timescales for fuel destruction of Ne- and Si-burning as a function of temperature. These are burning phases initiated by photodisintegrations and therefore not density-dependent.

duce rare proton-rich stable isotopes of heavy elements. The relation to the so-called p-process is discussed e.g. in Woosley & Howard (1978), Rayet, Prantzos, & Arnould (1990), Howard, Meyer, & Woosley (1991), and Rayet et al. (1995).

3.2.3. Explosive O-Burning

Temperatures in excess of roughly $3.3 \times 10^9 \text{K}$ lead to a quasi-equilibrium (QSE) in the lower QSE-cluster which extends over the range $28 < A < 45$ in mass number, while the path to heavier nuclei is blocked by small Q-values and reaction cross sections for reactions out of closed shell nuclei with Z or $N=20$ (see already Woosley, Arnett, & Clayton 1973 or Hix & Thielemann 1997). A full NSE with dominant abundances in the Fe-group cannot be attained. The main burning products are ^{28}Si , ^{32}S , ^{36}Ar , ^{40}Ca , ^{38}Ar , and ^{34}S , while ^{33}S , ^{39}K , ^{35}Cl , ^{42}Ca , and ^{37}Ar have mass fractions of less than 10^{-2} . In zones with temperatures close to $4 \times 10^9 \text{K}$ there exists some contamination by the Fe-group nuclei ^{54}Fe , ^{56}Ni , ^{52}Fe , ^{58}Ni , ^{55}Co , and ^{57}Ni .

The abundance distribution within the QSE-cluster is determined by alpha, neutron, and proton abundances. Because electron captures during explosive processing are negligible, the original neutron excess stays unaltered and fixes the neutron to proton ratio. Under those conditions the resulting composition is dependent only on the alpha to neutron ratio at freeze-out. In an extensive study Woosley, Arnett, and Clayton (1973) noted that with a neutron excess η of 2×10^{-3} the solar ratios of $^{39}\text{K}/^{35}\text{Cl}$, $^{40}\text{Ca}/^{36}\text{Ar}$, $^{36}\text{Ar}/^{32}\text{S}$, $^{37}\text{Cl}/^{35}\text{Cl}$, $^{38}\text{Ar}/^{34}\text{S}$, $^{42}\text{Ca}/^{38}\text{Ar}$, $^{41}\text{K}/^{39}\text{K}$, and $^{37}\text{Cl}/^{33}\text{S}$ are attained within a factor of 2 for freeze-out temperatures in the range $(3.1 - 3.9) \times 10^9 \text{K}$. This is the typical neutron excess resulting from solar CNO-abundances, which are first transformed into ^{14}N in H-burning and then into ^{22}Ne in He-burning via $^{14}\text{N}(\alpha, \gamma)^{18}\text{F}(\beta^+)^{18}\text{O}(\alpha, \gamma)^{22}\text{Ne}$. Similar results were obtained earlier by Truran and Arnett (1970), while for lower values of the neutron excess (as expected for stars of lower metallicity) essentially only the alpha

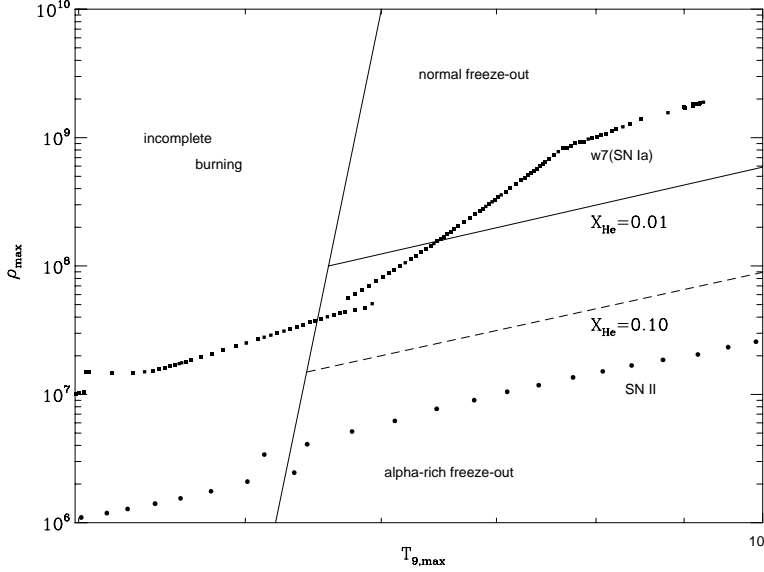


FIGURE 8. Division of the $\rho_{max}-T_{max}$ -plane for adiabatic expansions from ρ_{max} and T_{max} with an adiabatic index of 4/3 and a hydrodynamic timescale equal to the free fall timescale. Conditions separate into incomplete and complete Si-burning with normal and alpha-rich freeze-out. Contour lines of constant ${}^4\text{He}$ mass fractions in complete burning are given for levels of 1 and 10%. They coincide with lines of constant radiation entropy per gram of matter. For comparison also the maximum $\rho - T$ -conditions of individual mass zones in type Ia and type II supernovae are indicated.

nuclei ${}^{28}\text{Si}$, ${}^{32}\text{S}$, ${}^{36}\text{Ar}$, ${}^{40}\text{Ca}$ are produced in sufficient amounts (Truran and Arnett 1971). This affects element abundances and causes an odd-even staggering in Z .

3.2.4. Explosive Si-Burning

Zones which experience temperatures in excess of $4.0-5.0 \times 10^9 \text{K}$ undergo explosive Si-burning. For $T > 5 \times 10^9 \text{K}$ essentially all Coulomb barriers can be overcome and a nuclear statistical equilibrium is established. Such temperatures lead to complete Si-exhaustion and produce Fe-group nuclei. The doubly-magic nucleus ${}^{56}\text{Ni}$, with the largest binding energy per nucleon for $N=Z$, is formed with a dominant abundance in the Fe-group in case Y_e is larger than 0.49. Explosive Si-burning can be divided into three different regimes: (i) incomplete Si-burning and complete Si-burning with either (ii) a normal or (iii) an alpha-rich freeze-out. Which of the three regimes is encountered depends on the peak temperatures and densities attained during the passage of supernova shock front (see Fig. 20 in Woosley, Arnett, and Clayton 1973, and for applications to supernova calculations Fig. 4 in Thielemann et al. 1996b and Fig. 5 in Thielemann, Hashimoto, & Nomoto 1990 – combined here as Fig. 8). One recognizes that the mass zones of SNe Ia and SNe II experience different regions of complete Si-burning.

At high temperatures in complete Si-burning or also during a normal freeze-out, the abundances are in a full NSE and given by Eq.(3.31). An alpha-rich freeze-out is caused by the inability of the triple-alpha reaction ${}^4\text{He}(2\alpha, \gamma){}^{12}\text{C}$, transforming ${}^4\text{He}$ into ${}^{12}\text{C}$, and the ${}^4\text{He}(\alpha n, \gamma){}^9\text{Be}$ reaction, to keep light nuclei like n , p , and ${}^4\text{He}$, and intermediate mass nuclei beyond $A=12$ in an NSE during declining temperatures, when the densities

are small. The latter enter quadratically for these rates, causing during the fast expansion and cooling in explosive events a large alpha abundance after charged particle freeze-out, which shifts the QSE groups to heavier nuclei, transforming e.g. ^{56}Ni , ^{57}Ni , and ^{58}Ni into ^{60}Zn , ^{61}Zn , and ^{62}Zn . This also leads to a slow supply of carbon nuclei still during freeze-out, leaving traces of alpha nuclei, ^{32}S , ^{36}Ar , ^{40}Ca , ^{44}Ti , ^{48}Cr , and ^{52}Fe , which did not fully make their way up to ^{56}Ni . Figs. 9ab show this effect, typical for SNe II, as a function of remaining alpha-particle mass fraction after freeze-out. It is clearly seen that the major NSE nuclei ^{56}Ni , ^{57}Ni , and ^{58}Ni get depleted when the remaining alpha fraction increases, while all other species mentioned above increase.

Incomplete Si-burning is characterized by peak temperatures of $4 - 5 \times 10^9\text{K}$. Temperatures are not high enough for an efficient bridging of the bottle neck above the proton magic number $Z=20$ by nuclear reactions. Besides the dominant fuel nuclei ^{28}Si and ^{32}S we find the alpha-nuclei ^{36}Ar and ^{40}Ca being most abundant. Partial leakage through the bottle neck above $Z=20$ produces ^{56}Ni and ^{54}Fe as dominant abundances in the Fe-group. Smaller amounts of ^{52}Fe , ^{58}Ni , ^{55}Co , and ^{57}Ni are encountered. All explosive burning phases discussed above will be applied in more detail to SNe II nucleosynthesis in section 4.

3.2.5. *The r-Process*

The operation of an r-process is characterized by the fact that 10 to 100 neutrons per seed nucleus (in the Fe-peak or somewhat beyond) have to be available to form all heavier r-process nuclei by neutron capture. For a composition of Fe-group nuclei and free neutrons that translates into a neutron excess of $\eta = 0.4 - 0.7$ or $Y_e=0.15-0.3$. Such a high neutron excess can only be obtained through capture of energetic electrons (on protons or nuclei) which have to overcome large negative Q-values. This can be achieved by degenerate electrons with large Fermi energies and requires a compression to densities of $10^{11} - 10^{12}\text{g cm}^{-3}$, with a beta equilibrium between electron captures and β^- -decays (Cameron 1989) as found in neutron star matter (see also Meyer 1989).

Another option is an extremely alpha-rich freeze-out in complete Si-burning with moderate neutron excesses η and Y_e 's (0.16 or 0.42, respectively). After the freeze-out of charged particle reactions in matter which expands from high temperatures but relatively low densities, 70, 80, 90 or 95% of all matter can be locked into ^4He with $N=Z$. Figure 9 showed the onset of such an extremely alpha-rich freeze-out by indicating contour lines for He mass fractions of 1 and 10%. These contour lines correspond to $T_9^3/\rho=\text{const}$, which is proportional to the entropy per gram of matter of a radiation dominated gas. Thus, the radiation entropy per gram of baryons can be used as a measure of the ratio between the remaining He mass-fraction and heavy nuclei. Similarly, the ratio of neutrons to Fe-group (or heavier) nuclei (i.e. the neutron to seed ratio) is a function of entropy and permits for high entropies, with large remaining He and neutron abundances and small heavy seed abundances, neutron captures which proceed to form the heaviest r-process nuclei (Woosley & Hoffman 1992, Meyer et al. 1992, Takahashi et al. 1994, Woosley et al. 1994b, Hoffman et al. 1996, 1997).

A different situation surfaces for maximum temperatures below freeze-out conditions for charged particle reactions with Fe-group nuclei. Then reactions among light nuclei which release neutrons, like (α, n) reactions on ^{13}C and ^{22}Ne , can sustain a neutron flux. The constraint of having 10-100 neutrons per heavy nucleus, in order to attain r-process conditions, can only be met by small abundances of Fe-group nuclei. Such conditions were expected when a shock front passes the He-burning shell and enhances the $^{22}\text{Ne}(\alpha, n)$ reaction by orders of magnitude. However, Blake et al. (1981) and Cowan, Cameron, & Truran (1983) could show that this neutron source is not strong enough for an r-process in

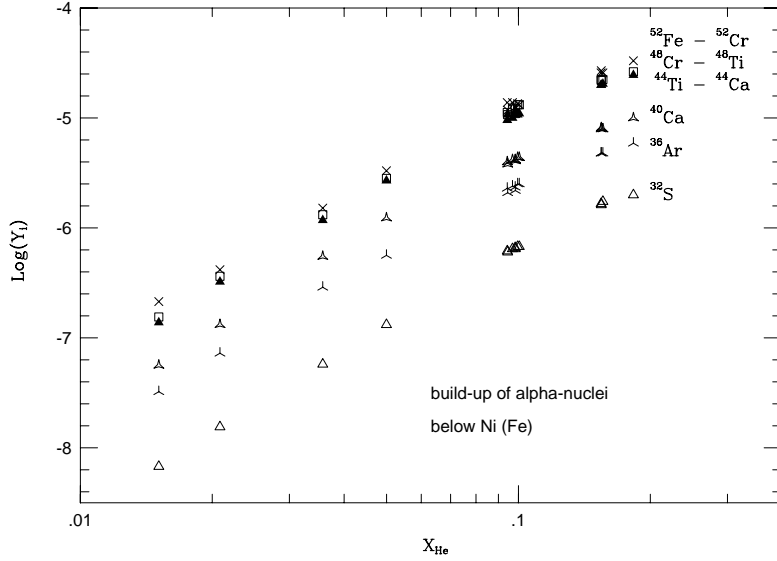
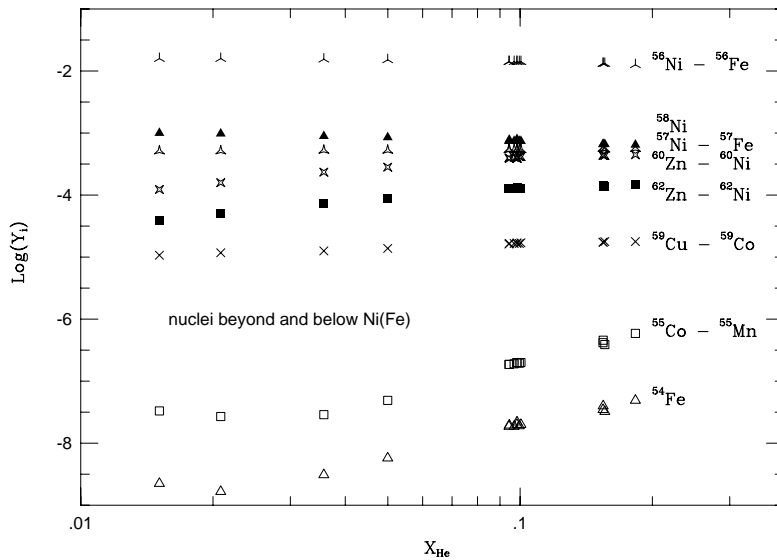


FIGURE 9. Display of the composition up to Cr and from Mn to Ni (after decay) as a function of remaining alpha mass-fraction X_{He} from an alpha-rich freeze-out. Lighter nuclei, being produced by alpha-captures from a remaining alpha reservoir, have larger abundances for more pronounced alpha-rich freeze-outs. Nuclei beyond Fe and Ni behave similarly, because of shifts in the dominant Fe-group nuclei caused by alpha-captures. Therefore, the dominant Fe-group nuclei like Fe and Ni show the opposite effect.



realistic stellar models (see also subsection 3.2.1). Recent research, based on additional neutron release via inelastic neutrino scattering (Epstein, Colgate, and Haxton 1988), can also not produce neutron densities which are required for such a process to operate (see also Woosley *et al.* 1990 and Meyer 1995).

r-process calculations independent of a specific astrophysical site, and just based on the goal to find the required neutron number densities and temperatures which can reproduce the solar abundance pattern of heavy elements, have been performed for a number of years. The latest ones are e.g. Kratz *et al.* (1988), Thielemann *et al.* (1993), Kratz *et al.* (1993), Thielemann *et al.* (1994a), Chen *et al.* (1995), Bouquelle *et al.* (1996), Pfeiffer, Kratz, & Thielemann (1997), Kratz, Pfeiffer, & Thielemann (1997) and Freiburghaus *et al.* (1997b). They, together with applications to the astrophysical sites listed above, will be discussed in section 5.

3.3. *Nucleosynthesis in Supernovae*

In the following section 4 we will apply these explosive burning processes to nucleosynthesis calculations in supernova explosions from massive stars (SNe II) for nuclei with $A < 70$. The discussion of the explosive production of heavier nuclei in supernovae will be given in section 5. There exist many original and review articles about the mechanisms of SNe II (e.g. Bruenn 1989ab, Cooperstein & Baron 1990, Wilson & Mayle 1988, Mayle & Wilson 1990, Bethe 1990, Bruenn & Haxton 1991; Wilson & Mayle 1993, Herant *et al.* 1994, Janka & Müller 1995,1996, Burrows 1996; Mezzacappa *et al.* 1997), so that we do not intend to repeat such a discussion here. We rather want to concentrate on the accompanying nucleosynthesis processes.

One of the major free parameters in stellar evolution, and thus for the pre-supernova models, is the still uncertain $^{12}\text{C}(\alpha, \gamma)^{16}\text{O}$ reaction (see Filippone, Humblet, & Langanke 1989, Caughlan *et al.* 1985, Caughlan and Fowler 1988, Barker & Kajino 1991, Buchmann *et al.* 1993, Zhao *et al.* 1993ab, Azuma *et al.* 1994, Langanke and Barnes 1996, Buchmann *et al.* 1996,1997). The permitted uncertainty range still spans almost over a factor of 3. However, also the treatment of convection in stellar evolution is not a settled one, especially the issue of overshooting and semiconvection. This has an influence on the possible growth of the He-burning core, which causes mixing in of fresh He at higher temperatures, and consequently also enhances the O/C ratio. Stellar evolution calculations by Langer and Henkel (1995) show that the total amount of ^{16}O can also vary by almost a factor of 3, for the extreme choices of the semi-convection parameter.

Thus, only the combination of these two uncertain parameters can be determined by comparison with abundance observations from supernova explosions. The calculations, presented in this review, are based on stellar models which made use of the Schwarzschild criterion of convection (Nomoto & Hashimoto 1988; Hashimoto *et al.* 1995) and employed the $^{12}\text{C}(\alpha, \gamma)^{16}\text{O}$ -rate by Caughlan *et al.* (1985), which is one choice within the permitted uncertainty window.

4. Type II Supernova Explosions

All stars with main sequence masses $M > 8M_{\odot}$ (e.g. Nomoto & Hashimoto 1988, Hashimoto, Iwamoto & Nomoto 1993, Weaver & Woosley 1993) produce a collapsing core after the end of their hydrostatic evolution, which proceeds to nuclear densities (for a review see e.g. Bethe 1990). The total energy released, $2\text{-}3 \times 10^{53}\text{erg}$, equals the gravitational binding energy of a neutron star. Because neutrinos are the particles with the longest mean free path, they are able to carry away that energy in the fastest fash-

ion. This was proven by the neutrino emission of supernova 1987A, detected in the Kamiokande, IMB and Baksan experiments (see Burrows 1990 for an overview).

The most promising mechanism for supernova explosions is based on neutrino heating beyond the hot proto-neutron star via the dominant processes $\nu_e + n \rightarrow p + e^-$ and $\bar{\nu}_e + p \rightarrow n + e^+$ with a (hopefully) about 1% efficiency in energy deposition (see also M. Guidry, this volume). The neutrino heating efficiency depends on the neutrino luminosity, which in turn is affected by neutrino opacities (e.g. Bruenn 1985, Sawyer 1989, Schinder 1990, Horowitz & Wehrberger 1992, Mezzacappa & Bruenn 1993, Keil & Janka 1995, Reddy & Prakash 1997, Reddy, Prakash, & Lattimer 1997). The explosion via neutrino heating is delayed after core collapse for a timescale of seconds or less. The exact delay time t_{de} depends on the question whether neutrinos diffuse out from the core (>0.5 s), weak convection occurs due to composition gradients, or convective turnover due to entropy gradients shortens this escape time substantially (e.g. Burrows & Fryxell 1992, Janka & Müller 1993, Wilson & Mayle 1993, Herant et al. 1994, Bruenn, Mezzacappa, & Dineva 1995, Janka & Müller 1995,1996, Burrows 1996; Mezzacappa et al. 1997). The behavior of t_{de} as a function of stellar mass is still an open question and quantitative results of self-consistent calculations should still be taken with care, suggesting instead to make use of the fact that typical kinetic energies of 10^{51} erg are observed and light curve as well as explosive nucleosynthesis calculations can be performed by introducing a shock of appropriate energy in the pre-collapse stellar model (see e.g. Woosley & Weaver 1986, Shigeyama, Nomoto & Hashimoto 1988, Thielemann, Hashimoto, & Nomoto 1990, Aufderheide, Baron, & Thielemann 1991, Weaver and Woosley 1993, Woosley & Weaver 1995, Thielemann, Nomoto, & Hashimoto 1996, Nomoto et al. 1997). Due to these remaining open questions, present explosive nucleosynthesis calculations for SNe II are still based on such induced supernova explosions by either depositing thermal energy or invoking a piston with a given kinetic energy of the order 10^{51} erg, in order to process and eject matter outside the collapsed Fe-core of a massive star.

These are not self-consistent calculations, which would also precisely determine a mass cut between the central neutron star and the ejected envelope. Although self-consistent calculations show promising results in recent years, on the one hand one expects changes from 2D to more realistic 3D calculations, on the other hand issues like the mass cut are not consistently solved yet, and some models would eject very unwanted nucleosynthesis products. Induced calculations, with the constraint of requiring ejected ^{56}Ni -masses from the innermost explosive Si-burning layers in agreement with supernova light curves, being powered by the decay chain ^{56}Ni - ^{56}Co - ^{56}Fe , are preferable at this point and can also serve as guidance to the solution of the whole supernova problem. Such mass cuts, based on ^{56}Ni in the ejecta, are always the "final" cuts, not necessarily the position of the high entropy bubble where neutrino heating causes the explosion. Massive stars will have some fallback, caused by reverse shocks reflected at density jumps in the outer layers. Recent observations of massive type II supernovae with very small amounts of ^{56}Ni are an indication for just this effect (Schmidt 1997, Turatto et al. 1997, Sollerman et al. 1998). Thus, when we will use the expression mass cut in the following, it will always relate to the final cut after fallback.

The composition of the innermost ejected layers is crucial and reflects aspects of the total energy in the shock and the temperatures attained due to it (responsible for ^{56}Ni), the neutronization of matter in form of Y_e , affecting the Fe-group composition in general and especially the $^{57}\text{Ni}/^{56}\text{Ni}$ ratio, and finally the entropy of the material which determines the degree of the alpha-rich freeze-out and with it the amount of some intermediate-mass alpha-elements like radioactive ^{44}Ti . Comparison with abundances from specific supernova observations or supernova remnants can teach a lot about these details and

the supernova mechanism as a function of progenitor mass. The amount of detected ^{16}O and ^{12}C or products from carbon and explosive oxygen burning can constrain our knowledge of the *effective* $^{12}\text{C}(\alpha, \gamma)^{16}\text{O}$ rate in He-burning. The $^{57}\text{Ni}/^{56}\text{Ni}$ ratio can give constraints on Y_e in the innermost ejected zones. This helps to estimate the necessary delay time between collapse and the neutrino-driven explosion. Provided that the stellar pre-collapse models are reliable, this allows additional insight into the exact working of the supernova explosion mechanism.

All these aspects can be explored when being guided by comparison to observations (e.g. SN1987A, a $20M_{\odot}$ during the main sequence stage – see e.g. Arnett et al. 1989, McCray 1993, Fransson & Kozma 1993, Suntzeff et al. 1992, 1997, Kozma & Fransson 1997; SN 1993J, a $14\pm 1M_{\odot}$ star during main sequence – see e.g. Nomoto et al. 1993, Shigeyama et al. 1994, Woosley et al. 1994a, Houck & Fransson 1996; type Ib and Ic supernova light curves like SN 1994I, which due to the lack of a large H-envelope and their early X-ray and gamma-ray losses are steeper than those of SNe II, but are also core collapse events – see e.g. Shigeyama et al. 1990, Nomoto et al. 1994, Iwamoto et al. 1994; the $^{57}\text{Ni}/^{56}\text{Ni}$ ratio deduced from γ -rays of the $^{56,57}\text{Co}$ decay or from spectral features changing during the decay time – see e.g. Clayton et al. 1992, Kurfess et al. 1992, Kumagai et al. 1993, Fransson & Kozma 1993, Varani et al. (1990); or supernova remnants like G292.0+1.8, N132D, CAS A – Hughes and Singh 1994, Blair et al. 1994, Iyudin et al. (1994), Dupraz et al. (1997), Hartmann et al. (1997); and comparison with abundances in low metallicity stars, which reflect the average SNe II composition (Wheeler, Sneden, & Truran 1989, Lambert 1989, Pagel 1991, Zhao & Magain 1990, Gratton & Sneden 1991, Edvardsson et al. 1993, Nissen et al. 1994, McWilliam et al. 1995, Schuster et al. 1996, Ryan, Norris, & Beers 1996, Norris, Ryan, & Beers 1996, Barbuy et al. 1997, Beers, Ryan, & Norris 1997, McWilliam 1997).

We concentrate here on the composition of the ejecta from such core collapse supernovae as an extension to earlier work (Hashimoto, Nomoto & Shigeyama 1989; Thielemann, Hashimoto & Nomoto 1990; Thielemann, Nomoto & Hashimoto 1993, 1994, 1996; Hashimoto et al. 1993, 1995; and Nomoto et al. 1997).

4.1. *Basic Nucleosynthesis Features*

The calculations were performed by depositing a total thermal energy of the order $E = 10^{51}\text{erg} +$ the gravitational binding energy of the ejected envelope into several mass zones of the stellar Fe-core. A first overview of results from the explosion calculations can be seen in Table 3 of Thielemann et al. (1996a) for element abundances and Table 1 of Nomoto et al. (1997) for isotopic abundances in the supernova ejecta as a function of progenitor star mass. They can be characterized by the following behavior: the amount of ejected mass from the unaltered (essentially only hydrostatically processed) C-core and from explosive Ne/C-burning (C, O, Ne, Mg) varies strongly over the progenitor mass range, while the amount of mass from explosive O- and Si-burning (S, Ar, and Ca) is almost the same for all massive stars. Si has some contribution from hydrostatic burning and varies by a factor of 2-3. The amount of Fe-group nuclei ejected depends directly on the explosion mechanism. The values listed for the $20M_{\odot}$ star have been chosen to reproduce the $0.07M_{\odot}$ of ^{56}Ni deduced from light curve observations of SN 1987A. The choice for the other progenitor masses is also based on supernova light curve observations, but their uncertain nature should be underlined and a clearer picture is only emerging now with the observation of varying amounts of ^{56}Ni for varying progenitor star masses (see Blanton, Schmidt, & Kirshner 1995, Schmidt 1997, Turatto et al. 1997, Sollerman, Cumming, & Lundquist 1998).

Thus, we have essentially three types of elements, which test different aspects of su-

pernovae, when comparing with individual observations. (i) The first set (C, O, Ne, Mg) tests the stellar progenitor models, (ii) the second (Si, S, Ar, Ca) the progenitor models and the explosion energy in the shock wave, while (iii) the Fe-group (beyond Ti) probes clearly in addition the actual supernova mechanism. Only when all three aspects of the predicted abundance yields can be verified with individual observational checks, it will be reasonably secure to utilize these results in chemical evolution calculations of galaxies (see e.g. Tsujimoto et al. 1995; Timmes et al. 1995; Pagel & Tautvaisiene 1995, 1997; Tsujimoto et al. 1997). In general we should keep in mind, that as long as the explosion mechanism is not completely and quantitatively understood yet, one has to assume a position of the mass cut which causes (not predicts!) a specific amount of ^{56}Ni ejecta. Dependent on that position, which is a function of the delay time between collapse and final explosion, the ejected mass zones will have a different neutron excess or $Y_e = \langle Z/A \rangle$ of the nuclear composition, determining the ratio $^{57}\text{Ni}/^{56}\text{Ni}$. The nature and amount of the energy deposition affects the entropy in the innermost ejected layers, and with it the degree of the alpha-rich freeze-out and amount of ^{44}Ti ejecta. We will discuss this in more detail in the following subsections.

4.2. *Ni(Fe)-Ejecta and the Mass Cut*

Figs. 10ab (both presenting a $13M_{\odot}$ star) make clear how strongly a Y_e change can affect the resulting composition. Fig. 10a makes use of a constant $Y_e=0.4989$ in the inner ejecta, experiencing incomplete and complete Si-burning. Figure 10b makes use of the original Y_e , resulting from the pre-collapse burning phases. Here Y_e drops to 0.4915 for mass zones below $M(r)=1.5M_{\odot}$. Huge changes in the Fe-group composition can be noticed. The change in Y_e from 0.4989 to 0.4915 causes a tremendous change in the isotopic composition of the Fe-group for the affected mass regions ($<1.5M_{\odot}$). In the latter case the abundances of ^{58}Ni and ^{56}Ni become comparable. All neutron-rich isotopes increase (^{57}Ni , ^{58}Ni , ^{59}Cu , ^{61}Zn , and ^{62}Zn), the even-mass isotopes (^{58}Ni and ^{62}Zn) show the strongest effect. In Fig. 10 one can also recognize the increase of ^{40}Ca , ^{44}Ti , ^{48}Cr , and ^{52}Fe with an increasing remaining He mass fraction. These are direct consequences of a so-called alpha-rich freeze-out with increasing entropy.

While these calculations were performed by depositing energy at a specific radius inside the Fe-core and letting the shock wave propagate outward, this should involve the outer structure of the star after collapse and at the time t_{de} , when the successful shock wave is initiated. Instead they were taken at the onset of core collapse, which would correspond to a prompt explosion without delay. In case of a delayed explosion, accretion onto the proto-neutron star will occur until finally after a delay period t_{de} a shock wave is formed, leading to the ejection of the outer layers. Aufderheide et al. (1991) performed a calculation with a model at $t_{de}=0.29\text{s}$ after core collapse for a $20M_{\odot}$ star, when the prompt shock had failed, and found an accretion caused increase of the mass cut by roughly $\Delta M_{acc}=0.02M_{\odot}$. A delayed explosion could set in after a delay of up to 1s, with the exact time being somewhat uncertain and dependent on the details of neutrino transport (Wilson & Mayle 1993, Herant et al. 1994, Bruenn, Mezzacapp, & Dineva 1995, Janka & Müller 1996, Burrows 1996).

The outer boundary of explosive Si-burning with complete Si-exhaustion is given by $T=5\times 10^9\text{K}$ and is also the outer boundary of ^{56}Ni production. From pure energetics it can be shown that this corresponds approximately to a radius $r_5=3700\text{ km}$ for $E_{SN}\approx 10^{51}\text{ erg}$, independent of the progenitor models (Woosley 1988, Thielemann, Hashimoto, & Nomoto 1990). Therefore, the mass cut would be at

$$M_{cut} = M(r_5) - M_{ej}(^{56}\text{Ni}). \quad (4.33)$$

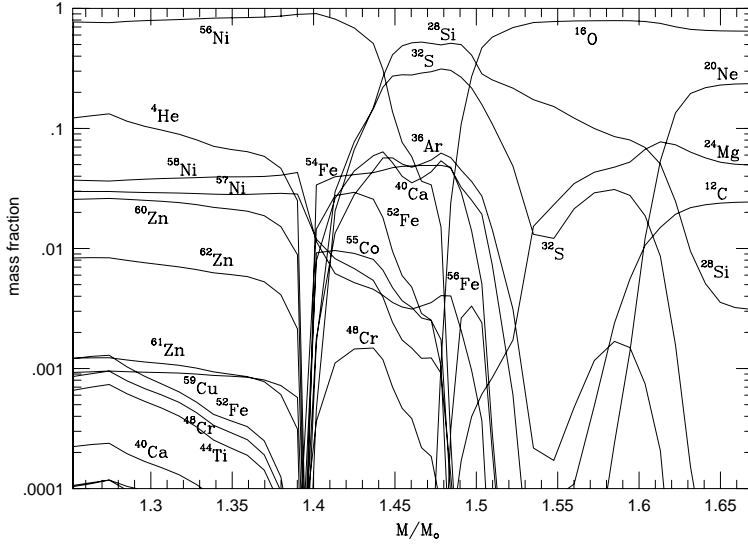
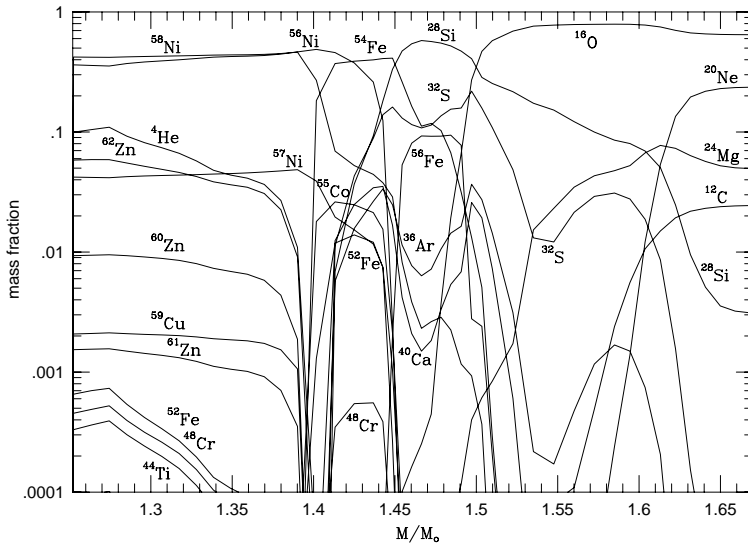


FIGURE 10. Isotopic composition of the ejecta for a core collapse supernova from a $13M_{\odot}$ star ($3.3M_{\odot}$ He-core). Only the dominant abundances of intermediate mass nuclei are plotted, while the Fe-group composition is presented in full detail. The exact mass cut in $M(r)$ between neutron star and ejecta depends on the details of the delayed explosion mechanism. Figures 10a and 10b show how strongly a Y_e -change can affect the resulting composition. Figure 10a makes use of a constant $Y_e=0.4989$ in the inner ejecta, Figure 10b makes use of the original Y_e , resulting from the pre-collapse burning phases, which drops to 0.4915 at the position for matter resulting from core O-burning, which experienced high densities and electron captures.



In case of a delayed explosion, we have to ask the question from which radius $r_{0,5}(t=0)$ matter fell in, which is located at radius $r_5(t=t_{de})=3700\text{km}$ when the shock wave emerges at time t_{de} . This effect of accretion as a function of delay time t_{de} has been studied in detail (Thielemann et al. 1996a). Here we want to present only the quantitative results.

In Figs. 11ab we display the Y_e -distributions of a 13 and a $20M_\odot$ star and the position of the outer boundary of explosive Si-burning with complete Si exhaustion, M_{ex-Si} , as a function of the delay time t_{de} . We consider for each star delay times of 0, 0.3, 0.5, 1, and 2s, resulting in $r_{0,5}=3700, 4042, 4412, 5410,$ and 7348km . Inside this boundary ^{56}Ni is produced as the dominant nucleus and the mass cuts would have to be positioned at $M_{cut}=M(r_{ex-Si}) - M_{ej}(^{56}\text{Ni})=M(r_{0,5}(0)) - M_{ej}(^{56}\text{Ni})$. When Ni-ejecta of 0.15 and $0.07M_\odot$ are used for 13 and $20M_\odot$ stars, mass cuts M_{cut} of 1.27 and $1.61M_\odot$ result for a vanishing delay time. For $t_{de,i}=0.3, 0.5, 1,$ and 2s the accreted masses $\Delta M_{acc,i}$ of 0.02, 0.03, 0.07-0.08, and $0.14-0.16M_\odot$ have to be added to M_{cut} . It is recognizable that especially for the $13M_\odot$ star the Y_e 's encountered for these different delay times vary strongly, and differences of the Fe-group composition can be expected. Assuming that the stellar models are correct, all delay times less than 1s for the $13M_\odot$ star are not compatible with the chemical evolution of our galaxy, as will be discussed below. On the other extreme, the Y_e in the innermost ejecta of a $25M_\odot$ star are not affected at all by the available choices. A more detailed discussion for the $20M_\odot$ star will follow.

The neutron star boundary would have to be moved outward, accordingly, by adding $\Delta M_{acc,i}$ mentioned in the previous paragraph. Whether a neutron star or black hole is formed depends on the permitted maximum neutron star mass, which is somewhat uncertain and related to the still limited understanding of the nuclear equation of state beyond nuclear densities (e.g. Glendenning 1991, Weber & Glendenning 1991, Brown & Bethe 1994, Prakash et al. 1997). A proto-neutron star with a baryonic mass M_b will release a binding energy E_{bin} in form of black body radiation in neutrinos during its contraction to neutron star densities. The gravitational mass is then given by

$$M_g = M_b - E_{bin}/c^2. \quad (4.34)$$

For reasonable uncertainties in the equation of state, Lattimer and Yahil (1989) obtained a relatively tight relation between gravitational mass and binding energy. Applying their expression results in a gravitational mass of the formed neutron star M_g . An error of roughly $\pm 15\%$ for the difference $M_b - M_g$ applies. ΔM_{acc} , due to the uncertainty of the accretion period or delay time, and the choice of $M_{ej}(^{56}\text{Ni})$ which determines M_{cut} , dominate the error in M_g of $1.16+(0-0.11)+(0.15-M_{ej}(^{56}\text{Ni}))$ for the example of the $13M_\odot$ star and $1.45+(0-0.12)+(0.07-M_{ej}(^{56}\text{Ni}))$ for the $20M_\odot$ and possible delay periods between 0 and 2s. The first bracket includes uncertainties in t_{de} , the second one in the actually ejected ^{56}Ni mass. A delay time of about 1s is expected to be an upper bound for the delayed explosions. This is close to a pure neutrino diffusion time scale without any convective turnover.

The results indicate a clear spread of neutron star masses. This spread would be preserved in real supernova events, unless a possible conspiracy in the combination of proto-neutron star masses, delay times, and explosion energetics (i.e. the explosion mechanism in general) leads to a smaller range in neutron star masses. A certain spread is also found in neutron star masses from observations (e.g. Nagase 1989, Page and Baron 1990, van Paradijs 1991, van Kerkwijk, van Paradijs, & Zuiderwijk 1995, van Paradijs & McClintock 1995, Thorsett 1996) but it is not clear to which extent it is just due to large observational errors. It is possible that the range predicted here already includes the

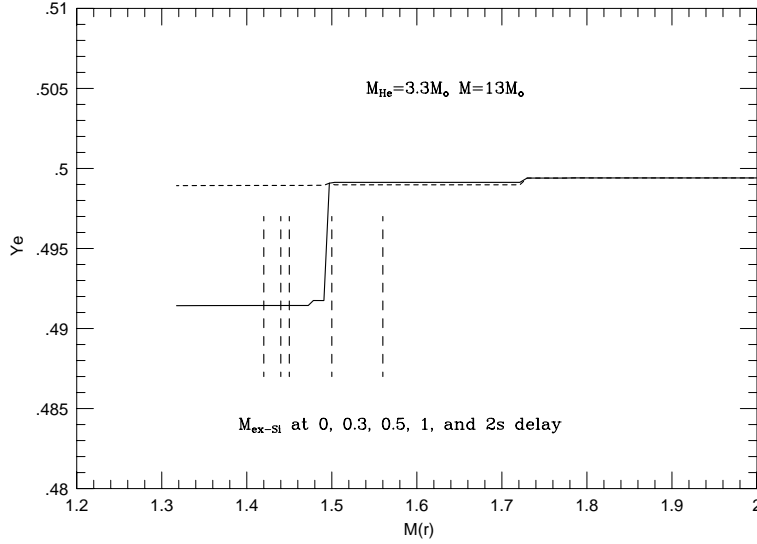
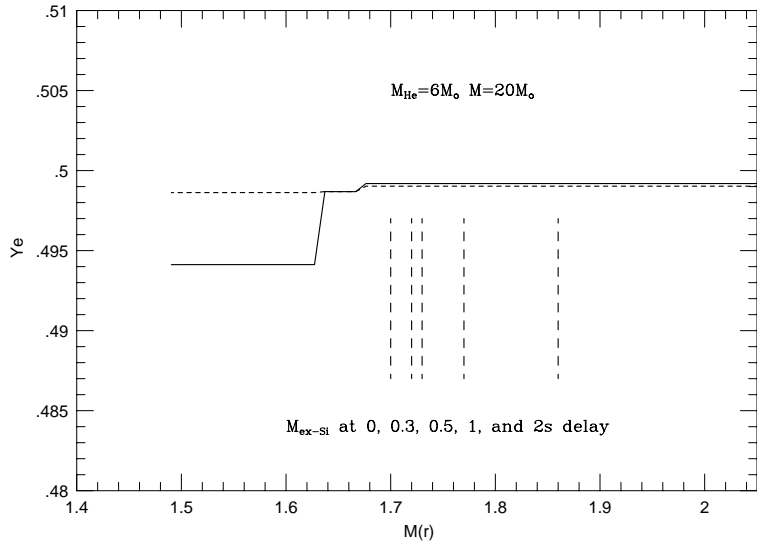


FIGURE 11. Figures 11ab present the Y_e -distributions of a 13 and $20M_{\odot}$ star and the position of the outer boundary of explosive Si-burning with complete Si-exhaustion, M_{ex-Si} , as a function of the delay/accretion period t_{de} . For each star delay times of 0, 0.3, 0.5, 1, and 2s are considered, resulting in $r_{0,5}$ =3700, 4042, 4412, 5410, and 7348km. ^{56}Ni is produced inside this boundary $r_{0,5}$ as the dominant nucleus. For a given amount of Ni-ejecta, mass cuts would have to be positioned at $M_{cut}=M(r_{ex-Si}) - M_{ej}(^{56}\text{Ni})=M(r_{0,5}(0)) - M_{ej}(^{56}\text{Ni})$. The delay times t_{de} and the required $M_{ej}(^{56}\text{Ni})$ determine Y_e in the ejected material (solid=original, dashed=experienced for sufficiently large t_{de} , when low Y_e -matter is accreted onto the neutron star. The step drop in Y_e corresponds to the edge of core O-burning.



uncertain upper mass limit of neutron stars due to the nuclear equation of state (Baym 1991, Weber and Glendenning 1991, Prakash et al. 1997). If it does, we would expect for these cases the formation of a central black hole during the delay period. Thus, no supernova explosion would occur and no yields be ejected. Different maximum stable masses between the initially hot and a cold neutron star (see e.g. Brown & Bethe 1994, Prakash et al. 1997 and the discussion of kaon condensates) could result in a supernova explosion *and* afterwards the formations of a central black hole. Timmes, Woosley, & Weaver (1996) had the stamina to predict a neutron star initial mass function based on ideas similar to the ones presented above. This is probably a somewhat bold undertaking, given the fact that we do not understand the supernova explosion mechanism fully, yet, and the ΔM_{acc} can vary widely. But there is one aspect which is worth mentioning. Due to the temperature dependence of the $^{12}\text{C}(\alpha, \gamma)^{16}\text{O}$ rate, stars above a critical mass limit will leave after core He-burning less than a critical amount of ^{12}C ($\approx 0.1M_{\odot}$), which leads to radiative rather than convective core C-burning and finally the formation of large Fe-cores, which probably form black holes rather than supernovae. This would also agree with observations based on the O/Fe ratio in early galactic evolution, which requires an upper mass limit of about 25-50 M_{\odot} in order to avoid too high a production of oxygen (Maeder et al. 1992, Tsujimoto et al. 1997).

4.3. *Observational Constraints*

There exist a number of quantitative comparisons for SN1987A (a 20 M_{\odot} star during its main sequence evolution) between nucleosynthesis predictions and observations [see e.g. Table 2 in Danziger et al. (1990), section IVb in Thielemann et al. (1990) or McCray (1993), Fransson, Houck, & Kozma (1996), Chugai (1994)], which show reasonable agreement for C, O, Si, Cl, Ar, Co, and Ni (or Fe) between observation and theory. We want to concentrate here on a crucial aspect, the O abundance.

The amount of ^{16}O is closely linked to the "effective" $^{12}\text{C}(\alpha, \gamma)^{16}\text{O}$ rate during core He-burning. This effective rate is determined by three factors: (1) the actual nuclear rate, (2) the amount of overshooting, mixing fresh He-fuel into the core at late phases of He-burning, when the temperatures are relatively high and favor alpha-captures on ^{12}C , and (3) the stellar mass or He-core size, which determine the central temperature during He-burning.

We have discussed above the nuclear rate and its uncertainties and used in Thielemann et al. (1996a) the rate by Caughlan et al. (1985) based on an astrophysical S-factor of $S_{tot}(0.3\text{MeV})=0.24\text{MeV barn}$. The S-factor is composed of an E1 component in the range 0.08 ± 0.020 and an E2-component with a much larger uncertainty of $0.066-0.064+0.104$ MeV barn, thus ranging in total from 0.062 to 0.270 MeV barn (the references where quoted in section 3). As the rate by Caughlan et al. (1985) seems to be close to the upper limit, it is crucial to check the observations for individual stellar models, in order to normalize the O-production correctly. The model calculations for a 20 M_{\odot} star predict 1.48 M_{\odot} of ejected ^{16}O . This is within observational constraints by Franson, Houck & Kozma (1993) who found about 1.5 M_{\odot} and Chugai (1994) who determined 1.2-1.5 M_{\odot} . It should, however, be clear that these observations test only the combined effect of nuclear rate and convection treatment (here Schwarzschild without overshooting). Similar results were found by Werner et al. (1995) when analyzing spectra of young white dwarfs with models of d'Antona and Mazzitelli (1992).

The O-determinations for SN 1993J from Houck & Fransson (1996) result in $\approx 0.5M_{\odot}$. Thielemann et al. (1996a) predicted 0.423 M_{\odot} for a 15 M_{\odot} main sequence star, which agrees fairly well, SN 1993J was determined to be a $14\pm 1M_{\odot}$ star. This leads to the conclusion that the Caughlan et al. (1985) rate, used in conjunction with the Schwarzschild

criterion for convection and no overshooting, gives a very good agreement with observations for individual supernovae. Only a comment about this combined usage can be made. Statements about the $^{12}\text{C}(\alpha, \gamma)^{16}\text{O}$ rate alone, in addition based on hydrostatic rather than explosive yields (Weaver & Woosley 1993) should be taken with some caution, and progress should preferably be made by improving nuclear cross sections and stellar convection treatment independently.

Recently other diagnostics became available for abundance determinations in supernova remnants. In that case the progenitor mass is not known, but the relative abundance ratios between different elements can be tested for consistency with abundance predictions for a variety of progenitor masses. Hughes and Singh (1994) made use of X-ray spectra of the supernova remnant G292.0+1.8 and found remarkable agreement for all element ratios from O through Ar with our $25M_{\odot}$ calculations (15% rms deviation). This tests implicitly the effective $^{12}\text{C}(\alpha, \gamma)^{16}\text{O}$ -rate, as it is also reflected in the ratios between C-burning products like Ne and Mg and explosive O-burning products like Ar and S. Comparisons with other model predictions (Woosley & Weaver 1995) led to larger deviations. UV and optical observations of supernova remnant N132D by Blair, Raymond & Long (1994) give very good agreement with our element predictions for a $20M_{\odot}$ star, with slight deviations for Mg. Thus, we have direct observations of supernovae and supernova remnants ranging from 15 over 20 to $25M_{\odot}$, which agree well with our model predictions and indicate that their application for other purposes should be quite reliable. This has recently also been demonstrated for galactic chemical evolution calculations (Tsujiimoto *et al.* 1995, 1997, Timmes, Woosley & Weaver 1995, Pagel & Tautvaisiene 1995, 1997).

The formation of the nuclei $^{58,61,62}\text{Ni}$, which are produced in form of the neutron-rich species ^{58}Ni and $^{61,62}\text{Zn}$, is strongly dependent on Y_e and varies therefore with the position of the mass cut between ejected matter and the remaining neutron star (see the discussion in Thielemann *et al.* 1990 and Kumagai *et al.* 1991, 1993). Especially for the Ni-abundances the position of the mass cut is crucial. The $^{57}\text{Ni}/^{56}\text{Ni}$ ratio is correlated with the abundances of stable Ni isotopes, predominantly ^{58}Ni , i.e. with $^{58}\text{Ni}/^{56}\text{Ni}$. Light curve observations of SN1987A (Elias *et al.* 1991, Bouchet *et al.* 1991, Suntzeff *et al.* 1992) could be interpreted with a high 57/56 ratio of 4 times solar, but this would also have required too large stable Ni abundances not substantiated from observations (Witteborn *et al.* 1989, Wooden *et al.* 1993, 1997). In order to meet the stable Ni constraints of $3\text{-}5 \times 10^{-3}M_{\odot}$ (Danziger *et al.* 1990, Witteborn *et al.* 1989, and Wooden *et al.* 1993) only an upper limit of 1.4-1.7 times solar is permitted for the 57/56 ratio from our results, given in detail in Thielemann *et al.* (1996). This also agrees well with the observations by Varani *et al.* (1990) and γ -ray line observations by GRO (Kurfess *et al.* 1992, Clayton *et al.* 1992). The apparent 57/56 discrepancy was solved by correct light curve and spectra modeling with a non-equilibrium treatment of the involved ionization stages at late times (Fransson & Kozma 1993). This gives a consistent picture for observations of stable Ni, light curve observations which are sensitive to ^{56}Co and ^{57}Co decay, and the γ -ray lines emitted from both decays.

This corresponds to a Y_e at the mass cut of 0.4987 within the little notch in Figure 11b. A mass cut at deeper layers, where Y_e decreases to 0.494, would imply 57/56 ratios larger than 2.5 times solar. A mass cut further out, implying a Y_e of 0.4989 results in a 57/56 ratio of the order of 1 times solar. This means that in order to meet the Y_e -constraint with an ejection of $0.075M_{\odot}$ of ^{56}Ni , we have a required delay time of 0.3-0.5s. Keeping all uncertainties of the model in mind, this can be taken as a support that SN 1987A did not explode via a prompt explosion, and did not experience a delayed explosion with a long delay time $t_{de} > 0.5\text{s}$. The latter would correspond more to a pure neutrino diffusion

case, while this result supports the understanding that larger neutrino luminosities are required than in the purely diffusive case (Herant et al. 1994; Burrows 1996; Janka & Müller 1996; Mezzacappa et al. 1997).

^{44}Ti is produced as a result of a strong alpha-rich freeze-out from explosive Si-burning, as discussed in section 3.2.4. Fig. 9 displays nicely that ^{44}Ti provides a measure of the entropy in the explosively processed matter. Exactly such conditions prevail in the innermost ejecta as can be seen in Figs. 10ab. Thus, we have another important observational constraint besides ^{56}Ni and ^{57}Ni , witnessing temperature, entropy and Y_e close to the mass cut. The predictions for ^{44}Ti ejecta range from 2×10^{-5} to $1.7 \times 10^{-4} M_\odot$ for stars ranging from 13 to 40 M_\odot (Woosley & Weaver 1995, Thielemann, Nomoto, & Hashimoto 1996, Nomoto et al. 1997). Observational limits for supernova remnants have been described in Timmes et al. (1996) and recent GRO, COMPTEL gamma-ray observations of CAS A (Iyudin et al. 1994, Dupraz et al. 1997, Hartmann et al. 1997) yield $(1.27 \pm 0.34 \times 10^{-4}) M_\odot$ with the new half life determinations between 59 and 62 y of Norman (1997), Görres et al. (1997), and Ahmad et al. (1997). This is a nice confirmation of nucleosynthesis predictions. Recent light curve calculations, based on the radioactive decay energies of ^{56}Ni , ^{57}Ni , and ^{44}Ti (Kozma & Fransson 1997), when compared with late time light curve observations of SN 1987A (Suntzeff et al. 1997), also come to the conclusion of $\approx 10^{-4} M_\odot$ ejecta of ^{44}Ti in good agreement with the predictions by Thielemann et al. (1996a), who obtained yields typically somewhat larger than Woosley & Weaver (1995), probably because energy deposition provides a somewhat larger entropy for the inner layers than induced explosions with the aid of a piston.

Unfortunately, we do not yet have similar observational and computational results for other supernovae. This would be a strong test for the explosion mechanism as a function of progenitor mass. It is important to explore the whole progenitor mass range with multidimensional explosion calculations in order to find out what Y_e and entropy self-consistent calculations would predict for the inner ejecta. Taken at face value, our 13 M_\odot model would ask for a delay time $> 1\text{s}$, in order to avoid pollution of the galaxy with an unwanted Fe-group composition.

A further test for the correct behavior of the ejecta composition as a function of progenitor mass is the comparison with abundances in low metallicity stars. These reflect the average SNe II composition, integrated over an initial mass function of progenitor stars. First individual tests were done in Thielemann et al. (1990, 1996a). Applications to full chemical evolution calculations of the galaxy were performed by e.g. Tsujimoto et al. (1995), Timmes et al. (1995), Pagel & Tautvaisiene (1995, 1997), and Tsujimoto et al. (1997) and prove to be a clear testing ground for supernova models. A verification of SNe II ejecta in such a way permits a correct application in chemical evolution calculations together with SNe Ia and planetary nebula ejecta (stars of initial mass $M < 8 M_\odot$ which form white dwarfs and eject their H- and He-burned envelopes).

5. The r-Process

The rapid neutron-capture process (r-process) leads to the production of highly unstable nuclei near the neutron drip-line and functions via neutron captures, (γ, n) -photodisintegrations, β^- -decays and beta-delayed processes. Neutrino-induced reactions may also play a possible role. The r-process abundances witness the interplay between nuclear structure far from beta-stability and the appropriate astrophysical environment. Observations of heavy elements in low metallicity stars with abundances of Fe/H being 1/1000 to 1/100 of solar give information about stellar surface abundances, which are the abundances of the interstellar gas from which stars formed early in galactic evolution.

Such observations show on the one hand an apparently completely solar r-process abundance pattern, at least for $A > 130$, indicating that during such early times in galactic evolution only r-process sources and no s-process sources contributed to the production of heavy elements (Snedden et al. 1996, Cowan et al. 1997). That is consistent with the picture discussed in section 3.1 of the s-process origin in low and intermediate mass stars, which set in only at evolution times $> 10^8$ y.

On the other hand, it is also recognized that the r-process abundances come in with a delay of $> 10^7$ y after Fe and O (Mathews, Bazan, & Cowan 1992), which excludes the higher mass SNe II as r-process sources, because such massive stars beyond $10\text{-}12M_{\odot}$ have shorter evolution times. The r-process has generally been associated with the inner ejecta of type II supernovae [see e.g. the reviews by Cowan et al. (1991) and Meyer (1994)], but also the decompression of neutron star matter was suggested by Lattimer et al. (1977), Meyer (1989), and Eichler et al. (1989) and is consistent with the above mentioned low metallicity observations. Both these environments provide or can possibly provide high neutron densities and high temperatures. Models trying to explain the whole r-process composition by low neutron density ($< 10^{20} \text{ cm}^{-3}$) and temperature ($< 10^9$ K) environments, like e.g. explosive He-burning in massive stars Thielemann et al. (1979), were clearly invalidated by Blake et al. (1981). The high entropy wind of the hot neutron star following type II supernova explosions has been suggested as a promising site for r-process nucleosynthesis by Woosley & Hoffman (1992), Woosley et al. (1994b), and Takahashi et al. (1994).

Actual r-process calculations usually followed two different approaches. Some studies, focusing mostly on nuclear physics issues far from stability, made use of a model-independent approach for the r-process as a function of neutron number densities n_n and temperatures T , extending for a duration time τ [see e.g. Kratz et al. (1988), Kratz et al. (1993), Thielemann et al. (1994a), Chen et al. (1995), Bouquelle et al. (1996), Pfeiffer et al. (1997), and Kratz et al. (1997)]. Other studies usually stayed closer to a specific astrophysical environment and followed the expansion of matter on expansion timescales τ with an initial entropy S , passing through declining temperatures and densities until the freeze-out of all reactions [see e.g. Woosley and Hoffman (1992), Meyer et al. (1992), Howard et al. (1993), Hoffman et al. (1996), Qian & Woosley (1996), Hoffman et al. (1997), Meyer & Brown (1997ab), and Surman et al. (1997)]. Here we compare the similarities and differences between the two approaches and whether there actually exists a one-to-one relation. Special emphasis is given to constraints, resulting from a comparison with solar r-process abundances in either approach, on nuclear properties far from stability. In addition, investigations are presented to test whether some features can also provide clear constraints on the permitted astrophysical conditions. This relates mostly to the $A < 110$ mass range, where the high entropy scenario in supernovae faces problems.

5.1. *Model-Independent Studies*

The sequence of neutron captures, (γ, n) -photodisintegrations and beta-decays (and possibly additional reactions like beta-delayed neutron emission, fission etc.) have in principle to be followed with a detailed reaction network, given by a system of (several thousand) coupled differential equations with a dimension equal to the number of isotopes. This can be done efficiently, as shown in Cowan et al. (1991), however, approximations are also applicable for neutron densities and temperatures well in excess of $n_n > 10^{20} \text{ cm}^{-3}$ and $T > 10^9$ K, which cause reaction timescales as short as $\approx 10^{-4}$ s [see Cameron et al. (1983), Bouquelle et al. (1996), and Goriely & Arnould (1996)]. As the beta-decay half-lives are longer, roughly of the order of 10^{-1} s to a few times 10^{-3} s, an

equilibrium can set in for neutron captures and photodisintegrations. Such conditions allow to make use of the "waiting point approximation", sometimes also called the "canonical r-process", which is equivalent to an $(n, \gamma) - (\gamma, n)$ -equilibrium [$n_n \langle \sigma v \rangle_{n, \gamma}^{Z, A} Y_{(Z, A)} = \rho N_A \langle \sigma v \rangle_{n, \gamma}^{Z, A} Y_n Y_{(Z, A)} = \lambda_{\gamma, n}^{Z, A+1} Y_{(Z, A+1)}$, see Eq.(1.11)] for all nuclei in an isotopic chain with charge number Z . As the photodisintegration rate $\lambda_{\gamma, n}^{Z, A+1}$ is related to the capture rate $\langle \sigma v \rangle_{n, \gamma}^{Z, A}$ by detailed balance and proportional to the capture rate times $\exp(-Q/kT)$, as shown in Eq.(1.7), the maximum abundance in each isotopic chain (where $Y_{(Z, A)} \approx Y_{(Z, A+1)}$) is located at the same neutron separation energy S_n , being the neutron-capture Q -value of nucleus (Z, A) . This permits to express the location of the "r-process path", i.e. the contour lines of neutron separation energies corresponding to the maximum in all isotopic chains, in terms of the neutron number density n_n and the temperature T in an astrophysical environment, when smaller effects like ratios of partition functions are neglected, as reviewed in Cowan *et al.* (1991).

The nuclei in such r-process paths, which are responsible for the solar r-process abundances, are highly neutron-rich, unstable, and located 15 – 35 units away from β -stability with neutron separation energies of the order $S_n = 2 - 4$ MeV. These are predominantly nuclei not accessible in laboratory experiments to date. The exceptions in the $A = 80$ and 130 peaks were shown in Kratz *et al.* (1988) and Kratz *et al.* (1993) and continuous efforts are underway to extend experimental information in these regions of the closed shells $N=50$ and 82 with radioactive ion beam facilities. The dependence on nuclear masses or mass model predictions enters via S_n . The beta-decay properties along contour lines of constant S_n towards heavy nuclei [see e.g. Fig. 4 in Thielemann *et al.* (1994a) or Fig. 12 below for the region around the $N=82$ shell closure] are responsible for the resulting abundance pattern. The build-up of heavy nuclei is governed within the waiting point approximation only by effective decay rates λ_{β}^Z of isotopic chains. Then the environment properties n_n and T (defining the S_n of the path), and the duration time τ , predict the abundances. In case the duration time τ is larger than the longest half-lives encountered in such a path, also a steady flow of beta-decays will follow, making the abundance ratios independent of τ ($\lambda_{\beta}^Z Y_{(Z)} = \text{const.}$ for all Z 's, where $Y_{(Z)}$ is the total abundance of an isotopic chain and λ_{β}^Z its effective decay rate).

One has to recognize a number of idealizations in this picture. It assumes a constant $S_n(n_n, T)$ over a duration time τ . Then the nuclei will still be existent in form of highly unstable isotopes, which have to decay back to beta-stability. In reality n_n and T will be time-dependent. As long as both are high enough to ensure the waiting point approximation, this is not a problem, because the system will immediately adjust to the new equilibrium and only the new $S_n(n_n, T)$ is important. The prominent question is whether the decrease from equilibrium conditions in n_n and T (neutron freeze-out), which initially ensure the waiting point approximation, down to conditions where the competition of neutron captures and beta-decays has to be taken into account explicitly, will affect the abundances strongly. In our earlier investigations we considered a sudden drop in n_n and T , leading to a sudden "freeze-out" of this abundance pattern, and only beta-decays and also beta-delayed properties [neutron emission and fission] have to be taken into account for the final decay back to stability [see e.g. the effect displayed in Fig. 9 of Kratz *et al.* (1993)].

When following this strategy, the analysis of the solar-system isotopic r-process abundance pattern showed that a minimum of three components with different S_n 's, characterizing different r-process paths, was necessary for correctly reproducing the three peaks at $A \simeq 80, 130,$ and 195 and the abundances in between [Thielemann *et al.* (1993a), Kratz *et al.* (1993)]. The "low-A wings" of the peaks (when making use of experimen-

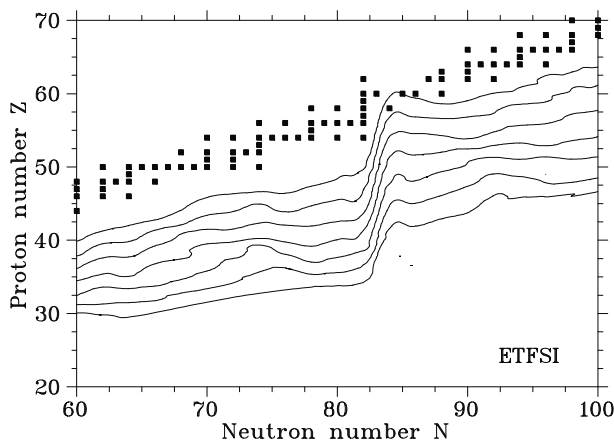


FIGURE 12. Contour plots of constant neutron separation energies $S_n=1,2,3,4,5,6$, and 7 MeV in the $80 \leq A \leq 140$ mass region for the ETFSI mass model Aboussir et al. (1995). The saddle point behavior before the shell closure at $N = 82$, also existing when using the FRDM masses by Möller et al. (1995), causes a deep trough before the peak at $A = 130$ (see upper part of Fig. 13), as the step from the abundance maximum of an isotopic chain Z to $Z+1$ can also cause a large jump in N or equivalently A , leading to a large number of unpopulated mass numbers A .

tal beta-decay properties at the magic neutron numbers $N = 50$ and 82), as well as the abundance pattern down to the next peak, could be reproduced, even with the assumption of a steady flow of beta-decays. This indicates that the astrophysical duration timescales τ are large in comparison to most of the beta-decay half-lives encountered and only comparable to the longest half-lives in the peaks (where the path comes closest to stability, see e.g. a 2 MeV contour line in Fig. 12), which control the leaking out to larger A 's. A continuous superposition of components with varying n_n , T or $S_n(n_n, T)$ (rather than only three), as expected in an astrophysical environment, with equidistant steps in S_n between 2 and 4 MeV and τ between 1 and 2.5 s led to a slight, but not dramatic, change/improvement of the abundance curve in Kratz et al. (1994).

When the calculations of Kratz et al. (1993) were supplemented by use of the most modern mass formula data [Finite Range Droplet Model FRDM by Möller et al. (1995) and Extended Thomas-Fermi model with Strutinski Integral ETFSI by Aboussir et al. (1995), instead of using a somewhat dated but still very successful droplet model by Hilf, von Groote, & Takahashi (1976), we could show that abundance troughs appeared before (and after) the 130 and 195 abundances peaks, due to the behavior of the S_n contour lines of these mass models [Thielemann et al. (1994a), Chen et al. (1995)]. The location in N of an r-process path with a given S_n does not behave smoothly as a function of Z . Fig. 12 indicates a sudden jump to the position of the magic neutron number, where the contour lines show a saddle point behavior for the FRDM as well as ETFSI mass models. The population gap of nuclei as a function of A leads after decay to the abundance trough of Fig. 13. The upper part of Fig. 13 shows the abundance curve obtained with ETFSI [Aboussir et al. (1995)] nuclear masses and beta-decay properties from a quasi-particle random-phase approximation [QRPA, Möller et al. (1997)]. When using FRDM masses by Möller et al. (1995) instead of the ETFSI predictions, a similar picture is obtained as shown in Thielemann et al. (1994a) and Bouquelle et al. (1996).

Additional tests were performed in order to see how this pattern could be avoided with different nuclear structure properties far from stability. The problem could be resolved in Chen et al. (1995), if for very neutron-rich nuclei the shell gap at the magic

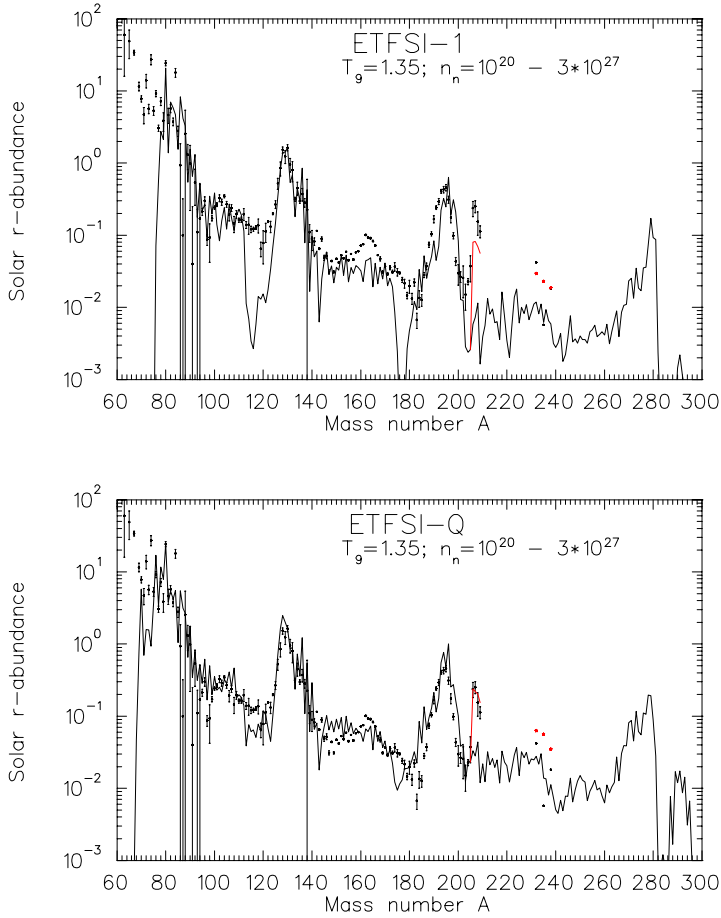


FIGURE 13. Fits to solar r-process abundances by Käppeler et al. (1989), obtained with 17 equidistant $S_n(n_n, T)$ components from 1 to 4 MeV. In the upper part, the result is presented for ETFSI masses with half-lives $\tau_{1/2}$ and beta-delayed neutron emission P_n values from QRPA calculations. In the lower part, the ETFSI-Q mass model by Pearson et al. (1996) was applied, which introduced a phenomenological quenching of shell effects, comparable to HFB calculations with the Skyrme force SkP of Dobaczewski, Nazarewicz, & Werner (1995). The quenching of the $N = 82$ shell gap leads to a filling of the abundance troughs and to a better overall reproduction of the heavy mass region. These results by Pfeiffer et al. (1997) are also the first which show a good fit to the r-process Pb and Bi contributions after following the decay chains of unstable heavier nuclei. For ^{232}Th , $^{235,238}\text{U}$ the solar and r-process production abundances are shown, allowing apparently for an increasing amount of decay with decreasing decay half-lives (in the sequence 232, 238, 235).

neutron number $N = 82$ is less pronounced, i.e. quenched, than predicted by the global macroscopic-microscopic mass models. In light nuclei, the quenching of shells in neutron-rich isotopes is well established and a long-studied effect [see Orr (1991), Campi et al. (1975), Fukunishi, Otsuka, & Sebe (1992), and Sorlin et al. (1993)]. The Hartree-Fock-Bogoliubov calculations by Werner et al. (1994), Dobaczewski et al. (1994), and Dobaczewski, Nazarewicz, & Werner (1995) with a specific Skyrme force had exactly the expected effect on the r-process path and the resulting abundance curve, as shown in Chen et al. (1995). This effect was recently also confirmed by Pearson et al. (1996), when the ETFSI mass formula was phenomenologically quenched in a similar way as the

HFB results and led to a very good agreement with solar r-abundances in a more systematic study by Pfeiffer *et al.* (1997) shown in the lower part of Fig. 13. An experimental investigation of shell quenching along the $N = 50$ and 82 shell towards more neutron-rich nuclei (and approaching the r-process path for $N = 126$) is a highly desirable goal in order to test the nuclear structure responsible for the solar abundances of heavy nuclei.

There are two aspects which have to be considered when trying to relate these simplified, model-independent results to astrophysics: (a) what kind of environments can produce the required conditions, and (b) do the nuclear structure conclusions drawn from the sudden freeze-out approximation stay valid for actual freeze-out timescales encountered in a specific environment? The second question cannot be answered in general, but only case by case. The question whether we understand fully all astrophysical sites leading to an r-process is not a settled one. There are strong indications that it is associated with type II supernovae. But galactic evolution timescales indicate that these can probably only be the low mass SNe II with longer evolution timescales Cowan *et al.* (1991), Mathews *et al.* (1992), while neutron star mergers or still other sites are not necessarily excluded Lattimer *et al.* (1977), Meyer (1989), Eichler *et al.* (1989).

5.2. Parameter Studies for High Entropies

5.2.1. The Model and Nuclear Input

Recent r-process studies by Woosley *et al.* (1994b), Takahashi *et al.* (1994), Qian & Woosley (1996), and Hoffman *et al.* (1997) have concentrated on the hot, neutron-rich environment in the innermost ejecta of type-II supernovae, also called the neutrino wind. These are the layers heated by neutrino emission and evaporating from the hot proto-neutron star after core collapse. These calculations obtain neutron separation energies of the r-process path S_n of 2 – 4 MeV, in agreement with the conclusions of section 5.1. Whether the entropies required for these conditions can really be attained in supernova explosions has still to be verified. In relation to the questions discussed in section 5.1, it also has to be investigated whether a sudden freeze-out is a good approximation to these astrophysical conditions. In order to test this, and how explosion entropies can be translated into n_n and T (or S_n) of the model independent approach, we performed a parameter study based on the entropy S and the total proton to nucleon ratio Y_e (which measures the neutron-richness of the initial composition), in combination with an expansion timescale (for the radius of a blob of matter) of typically 0.05 s as in Takahashi *et al.* (1994), and varied nuclear properties (i.e. mass models) like in section 5.1.

Thus, a hot blob of matter with entropy S , (i) initially consisting of neutrons, protons and some alpha-particles in NSE ratios given by Y_e , expands adiabatically and cools, (ii) the nucleons and alphas combine to heavier nuclei (typically Fe-group) with some neutrons and alphas remaining, (iii) for high entropies an alpha-rich freeze-out from charged-particle reactions occurs for declining temperatures, leading to nuclei in the mass range $A \approx 80 - 100$, and (iv) finally these remaining nuclei with total abundance Y_{seed} can capture the remaining neutrons Y_n and undergo an r-process. We chose a parameterized model for the expansion, essentially to introduce an expansion timescale, which makes these calculations independent of any specific supernova environment. But we will have to test later whether the expansion timescale employed is relevant to the supernova problem. The calculations were performed for a grid of entropies S and electron abundances Y_e ($S = 3, 10, 20, 30, \dots 390 k_B/\text{baryon}$ and $Y_e = 0.29, 0.31, \dots 0.49$). Neutron capture rates were calculated with the new version of the statistical model code SMOKER by Rauscher *et al.* (1997), discussed in section 2. The β^- -rates came from experimental data or QRPA calculation by Möller *et al.* (1997).

Different mass zones have different initial entropies, which leads therefore to a superposition of different contributions in the total ejecta. For each pair of parameters Y_e and S , the calculations were initially started with a full charged particle nuclear network up to Pd. After the α -rich freeze-out, an r-process network containing only neutron induced reactions and beta-decay properties followed the further evolution. The dynamical r-process calculations were performed in the way as described in Cowan, Thielemann, & Truran (1991) and Rauscher et al. (1994). The amount of subsequent r-processing depends on the available number of neutrons per heavy nucleus Y_n/Y_{seed} ($Y_{seed} = \sum_{A>4} Y_{(Z,A)}$). In Fig. 14a the Y_n/Y_{seed} -ratio is plotted in the (S, Y_e) -plane. A simple scaling with Y_e is clearly visible. Fig. 14b also shows that low Y_e -values would be one mean to avoid the very high entropies required to obtain large Y_n/Y_{seed} -ratios.

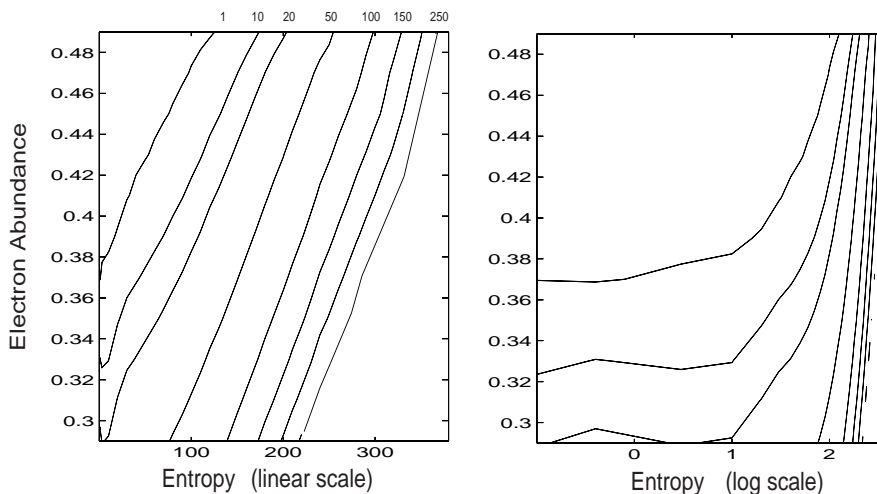


FIGURE 14. Y_n/Y_{seed} contour plots as a function of initial entropy S and Y_e for an expansion time scale of 0.05s, as expected from type II supernova conditions.

5.2.2. Superpositions of Entropies

The remaining question is, what kind of superposition of entropies the astrophysical environment provides. The calculations of Wittl et al. (1994) showed that the amount of mass ejected per entropy interval was relatively constant at late phases (when the higher entropy matter was expelled) and declining slightly at early phases (lower entropies) as a function of time (i.e. with increasing entropy). We did not perform complete hydro calculations, but rather followed these findings within a parametrized way, which allows to optimize for the best possible fit to the solar abundance distribution via a weighting function $g(S_i)$ with $g(S_i) = x_1 e^{-x_2 S_i}$, where i is the index of the components. We restrict ourselves here to two different Y_e -sequences with $Y_e=0.45$ and 0.49 shown in Fig. 15.

Entropies from about 200 to about 350 give Y_n/Y_{seed} -ratios growing from approximately 30 to 150. The α -rich freeze-out always produces seed nuclei in the range $90 < A < 120$. This material can then be “r-processed”, leading to a fully neutron dominated process as discussed in section 5.1 and the components have a very similar abundance pattern in the mass range $A = 110 - 200$. Thus, it is possible for this entropy range to establish a one-to-one correspondence for abundances obtained in r-process conditions between entropy and expansion timescale (S, τ) in one type of calculation and a neutron separation energy of the r-path and timescale $(S_n(n_n, T), \tau)$ in the calculations discussed in section 5.1. The neutron separation energy S_n of the r-path is the

one obtained during neutron capture freeze-out in the entropy based calculations. This correspondence can, however, only be established for entropies producing nuclei with $A > 110$.

Matter for $A < 110$ is a result of lower entropies with a neutron-poor and alpha-rich freeze-out, where the abundance of heavy nuclei is dominated by nuclei with alpha separation energies of ≈ 6 MeV and a $Z/A = Y_{e,heavy}$ of the dominating heavy nucleus after charged particle freeze-out, resulting from $Y_{e,global} = \sum_i Z_i Y_i \approx 0.5 X_\alpha + Y_{e,heavy} X_{heavy}$ with mass fractions $X_i = A_i Y_i$ [for more details see Freiburghaus *et al.* (1997ab)]. None of the entropies produces an abundance peak at charged particle freeze-out with $A < 80$, leaving a sufficient amount of neutrons for an r-processing which would reproduce the typical neutron-induced abundance features in the range $A = 80 - 110$. A different choice of $Y_{e,global}$ (shown here for 0.45 and 0.49) can influence that pattern somewhat in avoiding very large spikes for $A \approx 90$ and $N = 50$ isotopes, but the overall features stay.

Beyond $A = 110$ different mass models (in Fig. 15 only ETFSI is shown) give fits of similar quality as those displayed in section 5.1. The discrepancies below the $A = 130$ r-process peak, in form of a pronounced trough, occur again for the FRDM and ETFSI mass model. Thus, our results and conclusions from 5.1 can be translated also to "realistic" astrophysical applications for this mass region. The nuclear structure properties leading to agreement and deficiencies apply in the same way, due to the nature of a fast freeze-out, which preserves the abundances as they result from an initial $(n, \gamma) - (\gamma, n)$ -equilibrium at high temperatures, even when neutron captures and photodisintegrations are followed independently. Figure 16 shows the neutron number densities as a function of time. Low entropies ($S = 3 - 150$) that contribute to the mass range between $90 < A < 140$ lead to an r-process with a fast (almost sudden) freeze out on short timescales of $\tau \approx 0.04$ s. Thus it is not surprising that the trough before $A = 130$ (due to shell structure far from stability and its effect on abundance patterns in $(n, \gamma) - (\gamma, n)$ -equilibrium) survives.

There is possibly one difference to the conclusions given with Figure 13. As can be seen from Figure 16, the calculations experiencing the highest entropies have the longest neutron freeze-out timescales. On the other hand, they are responsible for the heaviest nuclei with the largest neutron capture cross sections. Our results show that the trough before the $A = 195$ peak, resulting in case of the ETFSI mass model and a waiting point approach, does not survive [see Thielemann *et al.* (1994a), Chen *et al.* (1995), Bouquelle *et al.* (1996), and Pfeiffer *et al.* (1997)]. This r-process abundance region is changed by ongoing (non-equilibrium) captures during the freeze-out and does not directly witness nuclear properties far from stability at the $N = 126$ shell closure. In Fig. 15 we actually observe a filling of the minimum before the $A = 195$ peak and even the ETFSI masses, that produced the largest trough in the waiting point calculations, seem to give a good fit.

There have been suggestions that neutrino-induced spallation of nuclei in the $A = 130$ peak, caused by the strong neutrino wind from the hot neutron star, could fill the abundance trough Qian *et al.* (1996). We refer to a more detailed discussion of this effect in Thielemann *et al.* (1997) and Freiburghaus (1997ab), including the requirements on neutrino luminosities and distances of matter from the neutron star at the time of the neutron freeze-out. We come to the conclusion that as an alternative interpretation the nuclear structure effects (shell quenching far from stability) outlined in detail in section 5.1 are still preferred, especially as they are already observed experimentally for lighter nuclei.

What can we learn from these entropy based studies and the fact that the r-process abundances below $A = 110$ cannot be reproduced correctly? There are several possible conclusions: (a) the high entropy wind is not the correct r-process site (on the one hand

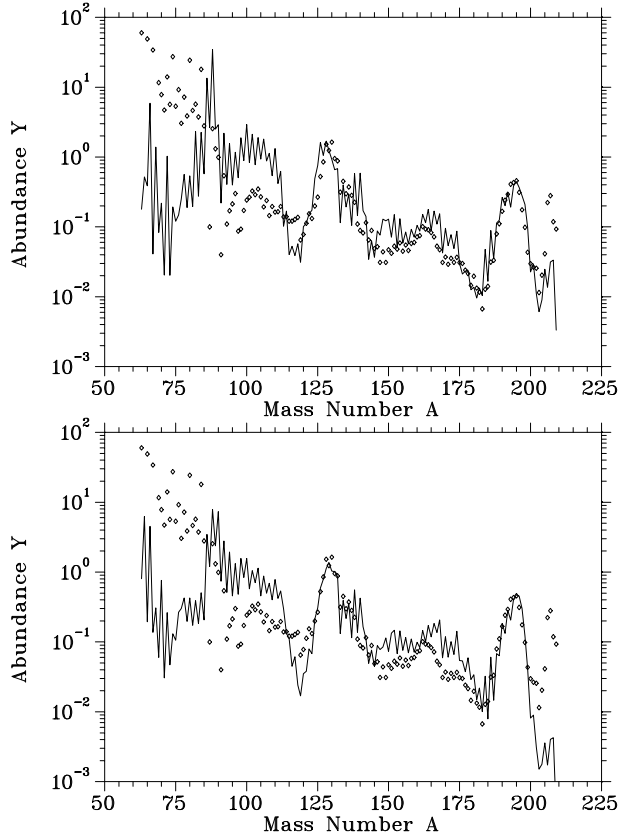


FIGURE 15. Similar to Fig 13 with the ETFSI mass formula, making use of a superposition of entropies $g(S)$ to attain an overall good fit to solar r-process abundances from the high entropy neutrino wind in type II supernovae. These calculations were performed with $Y_e = 0.45$, and 0.49 , but similar results are obtained in the range $0.30 - 0.49$, only requiring a scaling of entropy. The trough below $A = 130$ behaves similar to Fig. 13. This shows that a time dependent freeze-out (with a full treatment of neutron captures and photodisintegrations) resulting from a more realistic astrophysical scenario, can cause the same abundance deficiencies due to specific nuclear structure features as obtained in an instantaneous freeze-out from $(n, \gamma) - (\gamma, n)$ -equilibrium. The trough before the $A = 195$ peak existing e.g. for the ETFSI mass formula in the waiting point approximation and an instantaneous freeze-out is filled due to non-equilibrium freeze-out neutron captures. The strong deficiencies in the abundance pattern below $A = 110$ are due to the alpha-rich freeze-out and thus related to the astrophysical scenario rather than to nuclear structure.

due to the inherent deficiencies in the abundance pattern below $A = 110$ and the problems to obtain the high entropies in SNe II explosions, required for producing the massive r-process nuclei up to $A \simeq 195$ and beyond), or (b) the high entropy wind overcomes the problems to attain the high entropies and produces only the masses beyond $A = 110$, avoiding or diluting the ejection of the lower entropy matter. In the latter case another site is responsible for the lower mass region. An extension of Y_e to smaller values, as low as 0.3 , could also solve the problem, and constraints on ν_e and $\bar{\nu}_e$ fluxes and mean energies in the supernova environment have been explored by Qian & Woosley (1996) to achieve this goal. But in addition to a lower Y_e , also lower entropies are required as they might come from cold high density matter in beta-equilibrium (see section 3.2.5 and Cameron 1989, Meyer 1989, and Hillebrandt, Takahashi, & Kodama 1976). This can be

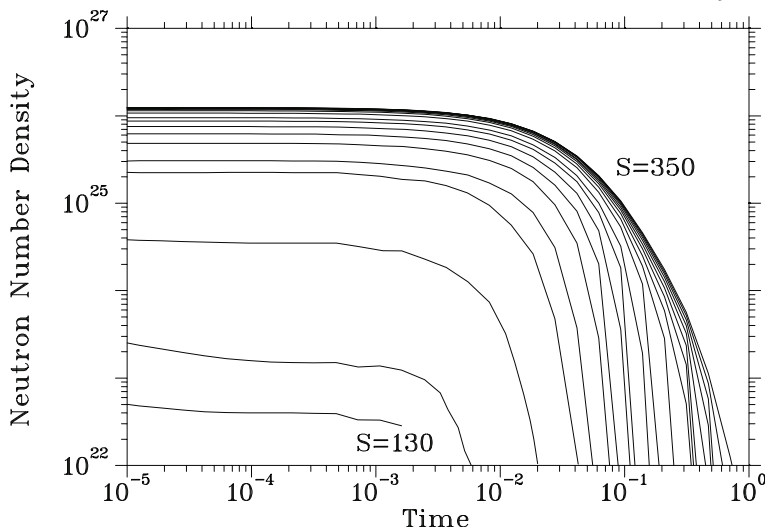


FIGURE 16. $n_n(t)$ in s, displayed for different entropies S in units of k_B per baryon.

deduced from Figure 14b. It shows the Y_n/Y_{seed} -ratio plotted in the (S, Y_e) -plane with a logarithmic entropy axis and extends down to entropies as low as $S = 10^{-2}$, where a normal and not an alpha-rich freeze-out is encountered.

Whether such an interpretation ($A < 130$ from low Y_e and S conditions, $A > 130$ from high S conditions) is the solution, might eventually be answered by observations. There seems to exist meteoritic evidence, discussed by Wasserburg et al. (1996), that the last r-process contributions to the solar system for $A > 130$ and $A < 130$ came at different times, i.e. from different types of events deduced from the extinct radioactivities ^{107}Pd , ^{129}I , and ^{182}Hf in meteoritic matter. It is highly desirable to have an independent verification of this from observations of low metallicity stars, which apparently show a completely solar r-process composition for nuclei with $A > 130$ [see Sneden et al. (1996), and Cowan et al. (1997)], possibly stemming from the first events in our galaxy which produce r-process nuclei (Mathews et al. 1992). It is also necessary to explore the abundances of nuclei with $A < 130$ in such observations, in order to test whether the solar pattern will also be found there or is absent, due to different evolution timescales of two independent stellar sources for these different mass ranges of r-process nuclei.

The results presented in this study benefitted from discussions with W.D. Arnett, R. Azuma, W. Benz, A. Burrows, S. Bruenn, J.J. Cowan, J. Dobaczewski, S. Goriely, C. Fransson, W. Hillebrandt, R. Hoffman, J. Hughes, H.-T. Janka, E. Kolbe, S. Kumagai, K. Langanke, J. Lattimer, A. Mezzacappa, P. Möller, E. Müller, M. Pearson, M. Prakash, Y.-Z. Qian, A. Ray, S. Reddy, B. Schmidt, R. Sawyer, F. Timmes, T. Tsujimoto, M. Turatto, P. Vogel, T. Weaver, and M. Wiescher. This work was supported by the Swiss Nationalfonds (grant 20-47252.96), the grant-in-Aid for Scientific Research (05242102, 06233101) and COE research (07CE2002) of the Ministry of Education, Science, and Culture in Japan, the German BMBF (grant 06Mz864) and DFG (grant Kr80615), the US NSF (grant PHY 9407194) and the Austrian Academy of Sciences. Some of us (FKT, CF, and KN) thank the ITP at the Univ. of California, Santa Barbara, for hospitality and inspiration during the supernova program.

REFERENCES

- Aboussir, Y., Pearson, J. M., Dutta, A. K., & Tondeur, F. 1995, *At. Data Nucl. Data Tables*, 61, 127
- Ahmad, I., Bonino, G., Castagnoli, G.C., Fischer, S.M., Kutschera, W., Paul, M. 1997, *Phys. Rev. Lett.*, submitted
- Alastuey, A., Jancovici, B. 1978, *Ap. J.* 226, 1034
- Arnett, W.D. 1995, *Ann. Rev. Astron. Astrophys.* 33, 115
- Arnett, W.D. 1996, *Nucleosynthesis and Supernovae*, Princeton Univ. Press
- Arnett, W.D., Bahcall, J.N., Kirshner, R.P., Woosley, S.E. 1989, *Ann. Rev. Astron. Astrophys.* 27, 629
- Arnett, W.D., Thielemann, F.-K. 1985, *Ap. J.* 295, 589
- Arnould, M., 1972, *A & A* 19, 92
- Arnould, M. 1997, *At. Data Nucl. Data Tables*, in press
- Audi, G., Wapstra, A.H. 1995, *Nucl. Phys. A595*, 409
- Aufderheide, M., Baron, E., Thielemann, F.-K. 1991, *Ap. J.* 370, 630
- Aufderheide, M., Fushiki, I., Woosley, S.E., Hartmann, D. 1994, *Ap. J. Suppl.* 91, 389
- Azuma, R. et al. 1994, *Phys. Rev. C50*, 1194
- Bao, Z. Y., Käppeler, F. 1987, *At. Data Nucl. Data Tables*, 36, 411
- Bao, Z. Y., Käppeler, F. 1997, private communication
- Baraffe, I., Bloemen, H., Borzov, I.N., Busso, M., Cooper, S., Dobaczewski, J., Durrer, R., von Feilitzsch, F., Gallino, R., Isern, J., Janka, H.-T., Lorenz, E., Pethick, C., Rolf, C., Thielemann, F.-K., Vervier, J., Wiescher, M. 1997, *NuPECC Report on Nuclear and Particle Astrophysics*, <http://quasar.physik.unibas.ch/nupecc>
- Barbuy, B. et al. 1997, *A & A* 317, L63
- Barker, F.C., Kajino, T. 1991, *Aust. J. Phys.* 44, 369
- Baym, G. 1991, in *Neutron Stars, Theory and Observations*, eds., J. Ventura and D. Pines, Kluwer Acad. Publ., Dordrecht, p.37
- Beer, H., Voss, F., Winters, R.R. 1992, *Ap. J. Suppl.* 80, 403
- Beers, T.C., Ryan, S.G., Norris, J.E. 1997, *Nucl. Phys. A621*, 37c
- Bethe, A.H. 1936, *Phys. Rev.* 50, 332
- Bethe, H.A. 1990, *Rev. Mod. Phys.* 62, 801
- Blair, W.P., Raymond, J.C., Long, K.S. 1994, *Ap. J.* 423, 334
- Blake, J.B., Woosley, S.E., Weaver, T.A., Schramm, D.N. 1981, *Ap. J.* 248, 315
- Blanton, E.L., Schmidt, B.P., Kirshner, R.P. 1995, *A. J.* 110, 2868
- Blatt, J.M., Weisskopf V.F. 1952, *Theoretical Nuclear Physics* Wiley, New York
- Borzov, I.N. 1996, *Z. Phys. A335*, 125; 1997, *Nucl. Phys. A621*, 307c
- Bouchet, P., Danziger, I.J. Lucy, L. 1991, in *SN1987A and Other Supernovae*, ed. I.J. Danziger (ESO, Garching), p. 217
- Bouquelle, V., Cerf, N., Arnould, M., Tachibana, M., Goriely, S. 1996, *A & A*, 305, 1005
- Brown, G.E., Bethe, H.A. 1994, *Ap. J.* 423, 659
- Brown, L.S., Sawyer, R.F. 1997, *Rev. Mod. Phys.* 69, 411
- Bruenn, S.W. 1985, *Ap. J. Suppl.* 58, 77
- Bruenn, S.W. 1989, *Ap. J.* 340, 955
- Bruenn, S.W. 1989, *Ap. J.* 341, 385
- Bruenn, S.W., Haxton, W.C. 1991, *Ap. J.* 376, 678
- Bruenn, S.W., Mezzacappa, A., Dineva, T. 1995, *Phys. Rep.* 256, 69
- Buchmann, L. et al. 1993, *Phys. Rev. Lett.* 70, 726
- Buchmann, L. 1996, *Ap. J.* 468, L127; 1997, *Ap. J.* 479, L153

- Buchmann, L., Azuma, R.E., Barnes, C.A., Humblet, J., Langanke, K. 1996, Phys. Rev. C54, 393; 1997, Nucl. Phys. A621, 153
- Burrows, A. 1990, Ann. Rev. Nucl. Part. Sci. 40, 181
- Burrows, A., Fryxell, B. 1992, Science 258, 430
- Burrows, A., Hayes, J., Fryxell, B. 1995, Ap. J. 450, 830
- Burrows, A., 1996, Nucl. Phys. A606, 151
- Cameron, A.G.W. 1989, in *Cosmic Abundances of Matter*, ed. C.J. Waddington, AIP Conf. Proc. 183, 349
- Cameron, A.G.W., Elkin, R.M. 1965, Can. J. Phys. 43, 1288
- Cameron, A.G.W., Cowan, J., Truran, J.W. 1983, Astropys. Space Sci., 91, 235
- Campi, X., Flocard, H., Kerman, A.K., Koonin, S. 1975, Nucl. Phys. A, A251, 193
- Caughlan, G.R., Fowler, W.A. 1988, At. Data Nucl. Data Tables, 40, 283
- Caughlan, G.R., Fowler, W.A., Harris, M.J., Zimmerman, G.E. 1985, At. Data Nucl. Data Tables 32, 197
- Chabrier, G., Schatzman, E. 1994, *The Equation of State in Astrophysics*, IAU Coll. 147, Cambridge Univ. Press
- Chaudhuri, A.K., Basu, D.N., Sinha, B. 1985, Nucl. Phys. A439, 415
- Chen, B., Dobaczewski, J., Kratz, K.-L., Langanke, K., Pfeiffer, B., Thielemann, F.-K., Vogel, P. 1995, Phys. Lett., B355, 37
- Chugai, N.N. 1994, Ap. J. 428, L17
- Clayton, D.D. 1968, 1983, *Principles of Stellar Evolution and Nucleosynthesis*, Univ. of Chicago Press
- Clayton, D.D., Leising, M.D., The, L.-S., Johnson, W.N., Kurfess, J.D. 1992, Ap. J. 399, L14
- Cooperstein, J., Baron, E. 1989, in *Supernovae*, ed. A. Petschek, Springer-Verlag, New York, p. 213
- Cowan, J.J., Cameron, A. G.W., Truran, J.W. 1983, Ap. J., 265, 429
- Cowan, J.J., McWilliam, A., Sneden, C., Burris, D.L. 1997, Ap. J., 480, 246
- Cowan, J. J., Thielemann, F.-K., Truran, J. W. 1991, Phy. Rep., 208, 267
- Danos, M. 1958, Nucl. Phys. 5, 23
- d'Antona, Mazzitelli, I. 1991, in IAU Symposium 145 *Evolution of Stars: The Photospheric Abundance Connection*, eds. G. Michaud, A. Tutukov, Kluwer Acad. Publ., Dordrecht, p.399
- Danziger, I.J., Bouchet, P., Gouiffes, C., Lucy, L. 1990, in *Supernovae*, ed S.E. Woosley, Springer-Verlag, New York, p.69
- Dean, D.J., Koonin, S.E., Langanke, K., Radha, P.B., Alhassid, Y. 1995, Phys. Rev. Lett. 74, 2909
- Dobaczewski, J., Hamamoto, I., Nazarewicz, W., Sheikh, J. A. 1994, Phys. Rev. Lett., 72, 981
- Dobaczewski, J., Nazarewicz, W., Werner, T. R. 1995, Phys. Scr., T56, 15
- Dupraz, C., Wessolowski, U., Oberlack, U., Georgii, R., Lichti, R., Iyudin, A., Schönfelder, V., Strong, A.W., Bloemen, H., Morns, D., Ryan, J., Winkler, C., Knödlseeder, J., von Ballmoos, P. 1997, A & A 324, 683
- Edvardsson, B., Andersen, J., Gustafsson, B. Lambert, D.L., Nissen, P.E., Tomkin, J. 1993, A & A 275, 101
- Eichler, D., Livio, M., Piran, T., Schramm, D. N. 1989, Nature, 340, 126
- Elias, J.H., Depoy, D.L., Gregory, B., Suntzeff, N.B. 1991, in *SN1987A and Other Supernovae*, ed. I.J. Danziger (ESO, Garching), p. 293
- Epstein, R.I., Colgate, S.A., Haxton, W.C. 1988, Phys. Rev. Lett. 61, 2038
- Ezhov, S.N., Plujko, V. A. 1993, Z. Phys. 346, 275
- Fantoni, S., Friman, B.L., Pandharipande, V.R. 1981, Phys. Rev. Lett. 48, 1089

- Filippone, B.W. 1987, *Ann. Rev. Nucl. Part. Sci.* 36, 717
- Filippone, B.W., Humblet, J., Langanke, K. 1989, *Phys. Rev.* C40, 515
- Fowler, W. A., Caughlan, G. E., Zimmermann, B. A. 1967, *Ann. Rev. Astron. Astrophys.* 5, 525
- Fowler, W.A., Caughlan, G.E., Zimmerman, B.A. 1975, *Ann. Rev. Astron. Astrophys.* 13, 69
- Fransson, C., Kozma, C. 1993, *Ap. J.* 408, L25
- Fransson, C., Houck, J., Kozma, C. 1996, in *IAU Coll. 145 Supernovae and SN Remnants*, ed. R. McCray, Cambridge Univ. Press, p.211
- Freiburghaus, C., Kolbe, E., Rauscher, T., Thielemann, F.-K., Kratz, K.-L., Pfeiffer, B. 1997, *Nucl. Phys.* A621, 405c
- Freiburghaus, C., Rembges, F., Rauscher, T., Kolbe, E., Thielemann, F.-K., Kratz, K.-L., Pfeiffer, B. 1997, *Ap. J.*, submitted
- Fukunishi, N., Otsuka, T., & Sebe, T. 1992, *Phys. Lett.*, B296, 279
- Fuller, G.M., Fowler, W.A., Newman, M. 1980, *Ap. J. Suppl.* 42, 447
- Fuller, G.M., Fowler, W.A., Newman, M. 1982, *Ap. J. Suppl.* 48, 279
- Fuller, G.M., Fowler, W.A., Newman, M. 1985, *Ap. J.* 293, 1
- Fuller, G., Meyer, B. S. 1995, *ApJ*, 453, 792
- Fushiki, I., Lamb, D.Q. 1987, *Ap. J.* 317, 368
- Gadioli, E., Hodgson, P. E., 1992, *Pre-Equilibrium Nuclear Reactions*, Clarendon Press, Oxford
- Gallino, R., Busso, M. 1997, in *Presolar Grains*, eds. T. Bernatowicz, E. Zinner, AIP, New York, p. xxx
- Gilbert, A., Cameron, A.G.W. 1965, *Can. J. Phys.* 43, 1446
- Glendenning, N.K. 1991, *Nucl. Phys.* B24B, 110
- Görres, J. et al. 1997, *Phys. Rev. Lett.*, submitted
- Görres, J., Wiescher, M., Thielemann, F.-K. 1995, *Phys. Rev.* C51, 392
- Goriely, S. 1996, *Nucl. Phys.* A605, 28
- Goriely, S., Arnould, M. 1996, *A & A*, 312, 327
- Gratton, R.G., Sneden, C. 1991, *A & A* 241, 501
- Hansen, J.P., Torrie, G.M., Veillefosse, P. 1977, *Phys. Rev.* A16, 2153
- Hartmann, D.H. et al. 1997, *Nucl. Phys.* A621, 83c
- Hashimoto, M., Iwamoto, K., Nomoto, K., 1993, *Ap.J.* 414, L105
- Hashimoto, M., Nomoto, K., Shigeyama, T. 1989, *A & A* 210, L5
- Hashimoto, M., Nomoto, K., Tsujimoto, T., Thielemann, F.-K. 1993, in *Nuclei in the Cosmos II*, ed. F. Käppeler, IOP Bristol, p.587
- Hashimoto, M., Nomoto, K., Thielemann, F.-K. 1995, in *Nuclei in the Cosmos III*, eds. M. Busso, R. Gallino, C. Raiteri, IOP, Bristol, p.419
- Hauser, W., Feshbach, H. 1952, *Phys. Rev. A* 87, 366
- Herant, M., Benz, W., Hix, W. R., Fryer, C.L., Colgate, S. A. 1994, *Ap. J.* 435, 339
- Hilf, E. R., von Groote, H., & Takahashi, K. 1976, in *Proceedings of the 3rd International Conference on Nuclei far from Stability*, Geneva, CERN-Rep 76-13, p.142
- Hillebrandt, W., Takahashi, K., and Kodama, T. 1976, *A & A* 52, 63
- Hirsch, M., Staudt, A., Muto, K., Klapdor-Kleingrothaus, H.V. 1992, *Nucl. Phys.* A535, 62
- Hix, W.R., Thielemann F.-K. 1996, *Ap. J.* 460, 869
- Hix, W.R., Thielemann F.-K. 1997, *Ap. J.*, submitted
- Hoffman, R. D., Woosley, S. E., Fuller, G. M., Meyer, B. S. 1996, *Ap. J.*, 460, 478
- Hoffman, R. D., Woosley, S. E., Qian, Y.-Z. 1997, *ApJ*, 482, 951
- Holmes, J.A., Woosley, S.E., Fowler, W.A., Zimmerman, B.A. 1976, *At. Data Nucl. Data Tables* 18, 306

- Horowitz, C.J., Wehrberger, K. 1992, Phys. Lett. B226, 236
- Houck, J.C., Fransson, C. 1996, Ap. J. 456, 811
- Howard, W. M., Goriely, S., Rayet, M., & Arnould, M. 1993, Ap. J., 417, 713
- Howard, W.M., Meyer, B.S., Clayton, D.D. 1992, Meteoritics 27, 404
- Howard, W.M., Meyer, B.S., Woosley, S.E. 1991, Ap. J. Lett. 373, L5
- Hughes, J.P., Singh, K.P. 1994, Ap.J. 422, 126
- Ichimaru, S. 1993, Rev. Mod. Phys. 65, 255
- Ichimaru, S. 1996, Publ. Astr. Soc. Japan 48, 613
- Ichimaru, S., & Utsumi, K. 1983, Ap. J. 269, L51
- Ichimaru, S., Tanaka, S., Iyetomi, H. 1984, Phys. Rev. A29, 2033
- Ichimaru, S., Utsumi, K. 1984, Ap. J. 286, 363
- Ignatyuk, A.V., Smirenkin, G.N., Tishin, A.S. 1975, Yad. Phys. 21, 485
- Ignatyuk, A.V., Istekov, K.K., Smirenkin, G.N. 1979, Sov. J. Nucl. Phys. 29, 450
- Ilijinov, A.S. et al. 1992, Nucl. Phys. A543, 517
- Itoh, N., Hayashi, H., Kohyama, Y. 1993; 1994, Ap. J. 418, 405; 436, 418
- Itoh, N., Hayashi, H., Nishikawa, A., Kohyama, Y. 1996, Ap. J. Suppl. 102, 411
- Itoh, N., Kuwashima, F., Munakata, H. 1990, Ap. J. 362, 620
- Itoh, N., Nishikawa, A., Kohyama, Y. 1996, Ap. J. 470, 1015
- Itoh, N., Totsuji, H., Ichimaru, S. 1977, Ap. J. 218, 477; Ap. J. 220, 742
- Itoh, N., Totsuji, H., Ichimaru, S., DeWitt, H.E. 1979, Ap. J. 234, 1079; Ap. J. 239, 415
- Itoh, M., Kumagai, S., Shigeyama, T., Nomoto, K., Nishimura, J. 1987 Nature 330, 233
- Iwamoto, K., Nomoto, K., Höflich, P., Yamaoka, H., Kumagai, S., Shigeyama, T. 1994, Ap. J. 437, L115
- Iyudin, A.F., Diehl, R., Bloemen, H., Hermsen, W., Lichti, G.G., Morns, D., Ryan, J., Schönfelder, V., Steinle, H., Varendorff, M., de Vries, C., Winkler, C. 1994, A&A 284, L1
- Janka, H.-T., Müller, E. 1993, in *Frontiers of Neutrino Astrophysics*, eds. Y. Suzuki, K. Nakamura, Universal Academy Press, Tokyo, p.203
- Janka, H.-T., Müller, E. 1995, Phys. Rep. 256, 135
- Janka, H.-T., Müller, E. 1996, A&A, 306, 167
- Jeukenne, J.P., Lejeune, A., Mahaux, C. 1977, Phys. Rev. C16, 80
- Käppeler, F., Beer, H., Wisshak, K. 1989, Rep. Prog. Phys. 52, 945
- Käppeler, F. et al. 1994, Ap. J. 437, 396
- Keil, W., Janka, H.-T. 1995, A & A 296, 145
- Kitamura, H., Ichimaru, S. 1995, Ap. J. 438, 300
- Klapdor, H.V., Metzinger, J., Oda, T. 1984, At Data Nucl. Data Tables 31, 81
- Kolbe, E., Krewald, S., Langanke, K., Thielemann, F.-K. 1992, Nucl. Phys. A540, 599
- Kolbe, E., Langanke, K., Krewald, S., Thielemann, F.-K. 1993, Phys. Rep. 227, 37
- Kolbe, E., Langanke, K., Thielemann, F.-K., Vogel, P. 1995, Phys. Rev. C52, 3437
- Kozma, C., Fransson, C. 1997, Ap. J., in press
- Kratz, K.-L. 1995, in AIP Conf. Proc. 327 of Nuclei in the Cosmos III, ed. M. Busso, R. Gallino, C. M. Raiteri, AIP Press, p.113
- Kratz, K.-L., Bitouzet, J.-P., Thielemann, F.-K., Möller, P., Pfeiffer, B. 1993, Ap. J. 402, 216
- Kratz, K.-L., Pfeiffer, B., Thielemann, F.-K., 1997, Nucl. Phys. A, in press
- Kratz, K.-L., Thielemann, F.-K., Hillebrandt, W., Möller, P., Harms, V., Truran, J. W. 1988, J. Phys. G, 14, 331
- Kratz, K.-L., Thielemann, F.-K., Möller, P., Pfeiffer, B. 1994, in Proc. 8th Int. Symp. on Capture

- Gamma-Ray Spectroscopy, ed. J. Kern, IOP Bristol, p.724
- Kumagai, S., Shigeyama, T., Hashimoto, M., Nomoto, K. 1991, *A & A* 243, L13
- Kumagai, S., Nomoto, K., Shigeyama, T., Hashimoto, M., Itoh, M. 1993, *A & A* 273, 153
- Kurfess, J. D. et al. 1992, *Ap. J.* 399, L137
- Lambert, D.L. 1989, in *Cosmic Abundances of Matter*, ed. C.J. Waddington, AIP Conf. Proc. 183, p.168
- Langanke, K., Barnes, C.A. 1996, *Adv. Nucl. Phys.* 22, 173
- Langanke, K., Vogel, P., Kolbe, E. 1996, *Phys. Rev. Lett.* 76, 2629
- Langer, N., Henkel, C 1995, in *Nuclei in the Cosmos III*, eds. M. Busso, R. Gallino, C.M. Raiteri, AIP Press, p.413
- Lattimer, J. M., Mackie, F., Ravenhall, D. G., Schramm, D. N. 1977, *Ap. J.*, 213, 225
- Lattimer, J.M., Yahil, A. 1989, *Ap. J.* 340, 426
- Lipparini, E., Stringari, S. 1989, *Phys. Rep.* 175, 103
- Maeder, A. 1992, *A & A* 264, 105
- Mahaux, C., 1982, *Phys. Rev.* C82, 1848
- Mahaux, C., Weidenmüller, H.A. 1979, *Ann. Rev. Part. Nucl. Sci.* 29, 1
- Malaney, R.A., Fowler, W.A. 1988, *Ap. J.* 333, 14
- Malaney, R.A., Fowler, W.A. 1989, *Ap. J.* 345, L5
- Mann, F.M. 1978, Hanford Engineering (HEDL-TME 78-83)
- Mathews, G.J., Bazan, G., Cowan, J.J. 1992, *Ap. J.* 391, 719
- Mayle, R. W., Wilson, J. R. 1990, in *Supernovae*, ed. S. E. Woosley, p.333
- McCray, R. 1993, *Ann. Rev. Astron. Astrophys.* 31, 175
- McFadden, L. Satchler, G.R., 1966, *Nucl. Phys.* 84, 177
- McWilliam, A. 1997, *Ann. Rev. Astron. Astrophys.* 35, 503
- McWilliam, A., Preston, G.W., Sneden, C., Searle, C. 1995, *A. J.* 109, 2757
- Mengoni, A., Nakajima, Y. 1994, *J. Nucl. Sci. Techn.* 31, 151
- Meyer, B. S. 1989, *Ap. J.*, 343, 254
- Meyer, B. S. 1994, *Ann. Rev. Astron. Astrophys.* 32, 153
- Meyer, B.S., 1995, *Ap. J.* 449, L55
- Meyer, B. S., Brown, J. S. 1997, *Nucl. Phys.* A621, 409c
- Meyer, B. S., Brown, J. S. 1997, *Ap. J. Suppl.* 112, 119
- Meyer, B.S., Mathews, G.J., Howard, W.M., Woosley, S.E., Hoffman, R.D. 1992, *Ap. J.* 399, 656
- Mezzacappa, A., Bruenn, S.W. 1993, *Ap. J.* 405, 637
- Mezzacappa, A., Calder, A.C., Bruenn, S.W., Blondin, J.M., Guidry, M.W., Strayer, M.R., Umar, A.S., 1997, *Ap. J.*, in press
- Michaud, G. Fowler, W.A. 1970, *Phys. Rev.* C2, 2041
- Michaud, G. Fowler, W.A. 1972, *Ap. J.* 173, 157
- Möller, P., Nix, J.R., Kratz, K.-L. 1997, *At. Data Nucl. Data Tables* 66, 131
- Möller, P., Nix, J.R., Myers, W.D., Swiatecki, W.J. 1995, *At. Data Nucl. Data Tables* 59, 185
- Möller, P., Randrup, J. 1990, *Nucl. Phys.* A514, 1
- Mohr, P., Rauscher, T., Oberhummer, H., Maté, Z., Fülöp, Zs., Somorjai, E., Jaeger, M., Staudt, G. 1997, *Phys. Rev.* C55, 1523
- Morgan, J.A. 1980, *Ap. J.* 238, 674
- Myers, W.D., Swiatecki, W.J., Kodama, T., El-Jaick, L.J., Hilf, E.R. 1977, *Phys. Rev.* C15, 2032
- Nagase, F. 1989, *Publ. Astron. Soc. Japan* 41, 1
- Nissen, P.E., Gustafsson, B., Edvardsson, B., Gilmore, G. 1994, *A & A* 285, 440

- Nomoto, K., Hashimoto, M. 1988, *Phys. Rep.* 163, 13
- Nomoto, K., Hashimoto, M., Tsujimoto, T., Thielemann, F.-K., Kishimoto, N., Kubo, Y., Nakasato, N. 1997, *Nucl. Phys.*, A161, 79c
- Nomoto, K., Suzuki, T., Shigeyama, T., Kumigai, S., Yamaoka, H., Saio, H. 1993, *Nature* 364, 507
- Nomoto, K., Thielemann, F.-K., Miyaji, S. 1985, *A & A* 149, 239
- Nomoto, K., Yamaoka, H., Pols, O. R., van den Heuvel, E. P. J., Iwamoto, K., Kumagai, S., Shigeyama, T. 1994, *Nature* 371, 227
- Norman, E.B. et al. 1997, *Phys. Rev. C*, submitted
- Oberhummer, H., Herndl, H., Rauscher, T., Beer, H. 1996, *Surveys in Geophys.* 17, 665
- Orr, N. A. 1991, *Phys. Lett.* B258, 29
- Paar, V. et al. 1997, in *Proc. Int. Conf. Gamma-Ray Spectroscopy and Related Topics*, ed. G. Molnar, Springer Hungarica, in press
- Page, D., Baron, E. 1990, *Ap. J.* 354, L17
- Pagel, B.E.J. 1991, *Phys. Scr.* T36, 7
- Pagel, B.E.J., Trautvaisiene, G., 1995, *MNRAS* 276, 505
- Pagel, B.E.J., Trautvaisiene, G., 1997, *MNRAS* 288, 108
- Pearson, J. M., Nayak, R. C., Goriely, S. 1996, *Phys. Lett.* B387, 455
- Pfeiffer, B., Kratz, K.-L. 1996, KCh Mainz Report, unpublished
- Pfeiffer, B., Kratz, K.-L., Thielemann, F.-K. 1997, *Z. f. Phys.* A357, 235
- Pichon, B. 1994, *Nucl. Phys.* A568, 553
- Prakash, M. et al. 1997, *Phys. Rep.* 280, 1
- Press, W.H., Flannery, B.P., Teukolsky, S.A., Vetterling, W.T. 1986, *Numerical Recipes*, Cambridge University Press
- Qian, Y.-Z., Vogel, P., Wasserburg, G.J. 1997, *Ap. J.*, submitted
- Qian, Y.-Z., Woosley, S. E. 1996, *Ap. J.*, 471, 331
- Qian, Y.-Z., Woosley, S.E., Haxton, W.C., Langanke, K., Vogel, P. 1996, *Phys. Rev.* C55, 1532
- Rauscher, T., Applegate, J.H., Cowan, J.J., Thielemann, F.-K., Wiescher, M. 1994, *Ap. J.*, 429, 499
- Rauscher, T., Thielemann, F.-K., Kratz, K.-L. 1997, *Phys. Rev.* C56, 1613
- Rauscher, T., Thielemann, F.-K. 1998, *At. Data Nucl. Data Tables*, to be published
- Rayet, M., Prantzos, N., Arnould, M. 1990, *A & A* 227, 211
- Rayet, M., Arnould, M., Hashimoto, M., Prantzos, N., Nomoto, K. 1995, *A & A* 298, 517
- Reddy, S., Prakash, M. 1997, *Ap. J.* 423, 689
- Reddy, S., Prakash, M., Lattimer, J.M. 1997, *Nucl. Phys. A*, submitted
- Reisdorf 1981, *Z. Phys.* A300, 227
- Ring, P., Schuck, P. 1980, *The Nuclear Many-Body Problem*, Springer-Verlag, Berlin
- Rolfs, C., Rodney, W.S. 1988, *Cauldrons in the Cosmos*, University of Chicago Press, Chicago
- Rolfs, C., Trautvetter, H.P., Rodney, W.S. 1987, *Rep. Prog. Phys.* 50, 233
- Ryan, S.G., Norris, J.E., Beers, T.C. 1996, *Ap. J.* 471, 254
- Salpeter, E.E., van Horn, H.M. 1969, *Ap. J.* 155, 183
- Satchler, G.R., Love, W.G. 1979, *Phys. Rep.* 55, 183
- Sawyer, R.F. 1989, *Phys. Rev.* C40, 865
- Schatz, H., Aprahamian, A., Görres, J., Wiescher, M., Rauscher, T., Rembges, J.F., Thielemann, F.-K., Kratz, K.-L., Pfeiffer, B., Möller, P., Herndl, B., Brown, B.A. 1997c, *Phys. Rep.*, in press
- Schinder, P.J. 1990, *Ap. J. Suppl.* 74, 249
- Schmidt, B.P. 1997, in *SN1987A: Ten Years After*, eds. M.M. Phillips, N.B. Suntzeff, *Astron.*

Soc. Pac., in press

- Schramm, S., Koonin, S.E. 1990, *Ap. J.* 365, 296
- Shigeyama, T., Nomoto, K., Hashimoto, M. 1988, *A & A* 196, 141
- Shigeyama, T., Nomoto, K., Tsujimoto, T., Hashimoto, M. 1990, *Ap. J.* 361, L23
- Shigeyama, T., Suzuki, T., Kumagai, S., Nomoto, K., Saio, H., Yamaoka, H., 1994, *Ap. J.* 420, 341
- Snedden, C., McWilliam, A., Preston, G. W., Cowan, J. J., Burris, D. I., Armosky, B. J. 1996, *Ap. J.* 467, 819
- Sollermann, J., Cumming, R.J., Lundquist, P. 1998, *Ap. J.* in press
- Sorlin, O. et al. 1993, *Phys. Rev.* C47, 2941
- Staudt, A., Bender, E., Muto, K., Klapdor, H.V. 1989, *Z. Phys.* A334, 47
- Staudt, A., Bender, E., Muto, K., Klapdor, H.V. 1990, *At. Data Nucl. Data Tables* 44, 79
- Suntzeff, N.B., Phillips, M.M., Elias, J.H., Walker, A.R., Depoy, D.L. 1992, *Ap. J.* 384, L33
- Suntzeff, N.B. et al. 1997, in *SN1987A: Ten Years After*, eds. M.M. Phillips, N.B. Suntzeff, *Astron. Soc. Pac.*, in press
- Surman, R., Engel, J., Bennett, J. R., Meyer, B. S. 1997, *Phys. Rev. C*, in press
- Sutaria, F.K., Sheikh, J.H., Ray, A. 1997, *Nucl. Phys.* A621, 375c
- Takahashi, K., Wittit, J., Janka, H.-T. 1994, *A&A*, 286, 857
- Takahashi, K., Yamada, M., Kondo, Z. 1973, *At. Data Nucl. Data Tables* 12, 101
- Takahashi, K., Yokoi, K. 1988, *At. Data Nucl. Data Tables* 36, 375
- Takahara, M., Nino, M., Oda, T., Muto, K., Wolters, A.A., Claudemans, P.W.M., Sato, K. 1989, *Nucl. Phys.* A504, 167
- Tepel, J.W., Hoffmann, H.M., Weidenmüller, H.A. 1974, *Phys. Lett.* B49, 1
- Thielemann, F.-K., Arnett, W.D. 1985, *Ap. J.* 295, 604
- Thielemann, F.-K., Arnould, M., Hillebrandt, W. 1979, *A & A*, 74, 175
- Thielemann, F.-K., Arnould, M., Truran, J. W. 1987, in *Advances in Nuclear Astrophysics*, ed. E. Vangioni-Flam, Gif sur Yvette, Editions Frontière, p.525
- Thielemann, F.-K., Arnould, M., Truran, J.W. 1988, *Capture Gamma-Ray Spectroscopy*, eds. K. Abrahams, P. van Assche, IOP, Bristol, p. 730.
- Thielemann, F.-K., Bitouzet, J.-P., Kratz, K.-L., Möller, P., Cowan, J. J., Truran, J. W. 1993, *Phys. Rep.*, 227, 269
- Thielemann, F.-K., et al. 1997, in *Capture Gamma-Ray Spectroscopy*, ed. G. Molnar, Springer Hungarica, in press
- Thielemann, F.-K., Hashimoto, M., Nomoto, K. 1990, *Ap. J.* 349, 222
- Thielemann, F.-K., Kratz, K.-L., Pfeiffer, B., Rauscher, T., van Wormer, L., & Wiescher, M. C. 1994, *Nucl. Phys.* A570, 329c
- Thielemann, F.-K., Metzinger, J., Klapdor, H.V. 1983, *Z. Phys.* A 309, 301
- Thielemann, F.-K., Nomoto, K., Hashimoto, M., 1993 in *Origin and Evolution of the Elements*, ed. N. Prantzos, E. Vangioni-Flam, M. Cassé, Cambridge Univ. Press, p.297
- Thielemann, F.-K., Nomoto, K., Hashimoto, M. 1994, in *Supernovae, Les Houches, Session LIV*, eds. S. Bludman, R. Mochkovitch, J. Zinn-Justin, Elsevier, Amsterdam, p. 629
- Thielemann, F.-K., Nomoto, K., & Hashimoto, M. 1996, *Ap. J.* 460, 408
- Thielemann, F.-K., Nomoto, K., Iwamoto, K., Brachwitz, F. 1996, in *Thermonuclear Supernovae*, eds. R. Canal, P. Ruiz-Lapuente, p. 485
- Thielemann, F.-K., Truran, J.W. 1987, in *Advances in Nuclear Astrophysics*, eds. E. Vangioni-Flam et al., Editions Frontières, Gif sur Yvette, p. 541
- Thomas, D., Schramm, D.N., Olive, K.A., Fields, B.D. 1993, *Ap. J.* 406, 569
- Thomas, D., Schramm, D.N., Olive, K.A., 1994, *Ap. J.* 430, 291
- Thomas, J., Zirnbauer, M.R., Langanke, K. 1986, *Phys. Rev.* C33, 2197

- Thorsett, S.E. 1996, Phys. Rev. Lett. 77, 1432 Phys. Rev. C33, 2197
- Timmes, F., Woosley, S.E., Weaver, T.A. 1995, Ap. J. Suppl. 98, 617
- Timmes, F., Woosley, S.E., Weaver, T.A. 1996, Ap. J. 457, 834
- Trimble, V. 1975, Rev. Mod. Phys. 47, 877
- Trimble, V. 1991, Astron. Astrophys. Rev. 3, 1
- Truran, J.W. 1972, Astrophys. Space Sci. 18, 308
- Truran, J.W. 1985, Ann. Rev. Nucl. Part. Sci. 34, 53
- Truran, J.W., Arnett, W.D. 1970, Ap. J. 160, 181
- Truran, J.W., Arnett, W.D. 1971, Astrophys. Space Sci. 11, 430
- Truran, J.W., Cameron, A.G.W., Gilbert, A. 1966, Can. J. Phys. 44, 563
- Truran, J.W., Cowan, J.J., Cameron, A.G.W. 1978, Ap. J. 222, L63
- Tsujimoto, T., Nomoto, K., Yoshii, Y., Hashimoto, M., Yanagida, S., Thielemann, F.-K. 1995, MNRAS 277, 945
- Tsujimoto, T., Yoshii, Y., Nomoto, K., Matteucci, F., Thielemann, F.-K. 1997, Ap. J. 483, 228
- Turatto, M. et al. 1997, in *SN1987A: Ten Years After*, eds. M.M. Phillips, N.B. Suntzeff, Astron. Soc. Pac., in press
- van Kerwijk, M.A., van Paradijs, J.A., Zuiderwijk, E.S. 1995, A& A 303, 497
- van Paradijs, J.A. 1991, in *Neutron Stars, Theory and Observations*, eds., J. Ventura and D. Pines, Kluwer Acad. Publ., Dordrecht, p.289
- van Paradijs, J.A., McClintock, J.E. 1995, in *X-Ray Binaries*, eds. W.H.G. Lewin, J. v. Paradijs, E.J.P. van den Heuvel, Cambridge Univ. Press, p. 111
- van Wormer, L., Görres, J., Iliadis, C., Wiescher, M., Thielemann, F.-K. 1994, Ap. J. 432, 267
- Varani, G.-F., Meikle, W.P.S., Spyromilio, J., Allen, D.A. 1990, MNRAS 245, 570
- Varner, R.L. Thompson, W.J., McAbee, T.L. Ludwig, E.J., Clegg, T.B. 1991, Phys. Rep. 201, 57
- Verbaatschot, J.J.M., Weidenmüller, H.A., Zirnbauer, M.R. 1984, Phys. Rep. 129, 367
- von Egidy, T., Behkami, A.N., Schmidt, H.H. 1986, Nucl. Phys. A376, 405
- von Egidy, T., Schmidt, H.H., Behkami, A.N. 1988, Nucl. Phys. A481, 189
- Wagoner, R.V. 1969, Ap. J. Suppl. 18, 247
- Wallerstein, G. et al. 1997, Rev. Mod. Phys. 69, 995
- Wang, R.-P., Thielemann, F.-K., Feng, D.H., Wu, C.-L. 1992, Phys. Lett. B284, 196
- Wasserburg, G., Busso, M., Gallino, R. 1996, Ap. J. 466, L109
- Weaver, T.A., Woosley, S.E. 1993, Phys. Rep. 227, 65
- Weber, F., Glendenning, N.K. 1991, Phys. Lett. B265, 1
- Werner K., Dreizler S., Heber U., Rauch T. 1995, *Nuclei in the Cosmos III*, eds. M. Busso, R. Gallino, C.M. Raiteri, AIP Press, p.45
- Werner, T. R., Sheikh, J. A., Nazarewicz, W., Strayer, M. R., Umar, A. S., Misu, M. 1994, Phys. Lett. B333, 303
- Wheeler, J.C., Sneden, C., Truran, J.W. 1989, Ann. Rev. Astron. Astrophys. 27, 279
- Wiescher, M., Görres, J., Thielemann, F.-K., Ritter, H. 1986, A & A 160, 56
- Wiescher, M., Harms, V., Görres, J., Thielemann, F.-K., Rybarczyk, L.J. 1987, Ap. J. 316, 162
- Wiescher, M., J. Görres 1988, Z. Phys. A329, 121
- Wiescher, M., Görres, J., Thielemann, F.-K. 1988, Ap. J. 326, 384
- Wiescher, M., Görres, J., Thielemann, F.-K. 1990, Ap. J. 363, 340
- Wiescher, M., Görres, J., Graaf, S, Buchmann, L., Thielemann, F.-K. 1989, Ap. J. 343, 352
- Wiescher, M., Steininger, R., Käppeler, F. 1989, Ap. J. 344, 464
- Wilson, J.R., Mayle, R.W. 1988, Phys. Rep. 163, 63

- Wilson, J.R., Mayle, R.W. 1993, Phys. Rep. 227, 97
- Wisshak, K., Voss, F., Käppeler, F., Kerzakov, I. 1997, Nucl. Phys. A621, 270c
- Witteborn, F.C., Bregman, J.D., Wooden, D.H., Pinto, P.A., Rank, D.M., Woosley, S.E., Cohen, M. 1989, Ap. J. 338, L9
- Witti, J., Janka, H.-T., Takahashi, K. 1994, A&A, 286, 841
- Wooden, D.H., Rank, D.M., Bregman, J.D., Witteborn, E.C., Cohen, M., Pinto, P.A., Axelrod, T.S. 1993, Ap. J. Suppl. 88, 477
- Wooden, D.H. 1997, in *Presolar Grains*, eds. T. Bernatowicz, E. Zinner, AIP, New York, p. xxx
- Woosley, S.E. 1988, Ap. J. 330, 218
- Woosley, S.E., Arnett, W.D., Clayton, D.D. 1973, Ap. J. Suppl. 26, 231
- Woosley, S.E., Fowler, W.A., Holmes, J.A., Zimmerman, B.A. 1978, At. Data Nucl. Data Tables 22, 371
- Woosley, S.E., Hartmann, D., Hoffman, R.D., Haxton, W.C. 1990, Ap. J. 356, 272
- Woosley, S. E., Hoffman, R. D. 1992, Ap. J. 395, 202
- Woosley, S.E., Howard, W.M. 1978, Ap. J. Suppl. 36, 285
- Woosley, S.E., Weaver, T.A. 1986, Ann. Rev. Astron. Astrophys. 24, 205
- Woosley, S.E., Eastman, R.G., Weaver, T.A., Pinto P.P. 1994, Ap. J. 429, 300
- Woosley, S.E., Weaver, T.A. 1994, in *Les Houches, Session LIV, Supernovae*, eds. S.R. Bludman, R. Mochkovitch, J. Zinn-Justin, Elsevier Science Publ., p. 63
- Woosley, S.E., Weaver, T.A. 1995, Ap. J. Suppl. 101, 181
- Woosley, S. E., Wilson, J. R., Mathews, G. J., Hoffman, R. D., Meyer, B. S. 1994, Ap. J. 433, 229
- Zhao, G., Magain, P. 1990, A & A 238, 242
- Zhao, Z., France, R.H., Lai, K.S., Rugari, S.L., Gai, M., Wilds, E.L. 1993, Phys. Rev. Lett. 70, 2066
- Zhao, Z., France, R.H., Lai, K.S., Rugari, S.L., Gai, M., Wilds, E.L., Kryger, R.A., Winger, J.A., Beard, K.B. 1993, Phys. Rev. C48, 429